

Article

Autonomous Minimum Safe Distance Maintenance from Submersed Obstacles in Ocean Currents

Timothy Sands ^{1,*} , Kevin Bollino ², Isaac Kaminer ³ and Anthony Healey ³¹ Department of Mechanical Engineering, Stanford University, Stanford, CA 94305, USA² Department of Electrical and Computer Engineering, George Mason University, Fairfax, VA 22030, USA; kbollino@gmu.edu³ Department of Mechanical and Aerospace Engineering, Naval Postgraduate School, Monterey, CA 93943, USA; kaminer@nps.edu (I.K.); healey@nps.edu (A.H.)

* Correspondence: dr.timsands@stanford.edu; Tel.: +1-3954-656-3954

Received: 27 June 2018; Accepted: 20 August 2018; Published: 22 August 2018

**Featured Application:** Submersed obstacle avoidance in unknown ocean currents via guidance, navigation, and control for autonomous underwater vehicles.

Abstract: A considerable volume of research has recently blossomed in the literature on autonomous underwater vehicles accepting recent developments in mathematical modeling and system identification; pitch control; information filtering and active sensing, including inductive sensors of ELF emissions and also optical sensor arrays for position, velocity, and orientation detection; grid navigation algorithms; and dynamic obstacle avoidance, amongst others. In light of these modern developments, this article develops and compares integrative guidance, navigation, and control methodologies for the Naval Postgraduate School's *Phoenix* submerged autonomous vehicle, where these methods are assumed available. The measure of merit reveals how well each of several proposed methodologies cope with known and unknown disturbances, such as currents that can be constant or harmonic, while maintaining a safe passage distance from underwater obstacles, in this case submerged mines. Classical pole-placement designs establish nominal baseline behaviors and are subsequently compared to performance of designs that are optimized to satisfy linear quadratic cost functions in regulators as well as linear-quadratic Gaussian designs. Feed-forward architectures and integral control designs are also evaluated. A noteworthy contribution is a very simple method to mimic optimal results with a "rule of thumb" criteria based on the design's time constant. Since the rule-of-thumb method uses the assumed system model for computation of the control, it is particularly generic. Cited references each contain methods for online system parameter identification (with a motivation of use in the finding the control signal), permitting the rule of thumb's generic applicability, since it is expressed in terms of the system parameters. This proposed method permits control design at sea where significant computation abilities are not available. Very simple waypoint guidance is also introduced to guide a vehicle along a preplanned path through a field of obstacles placed at random locations. The linear-quadratic Gaussian design proves best when augmented with integral control, and works well with reduced-order equations, while the "rule of thumb" design is seen to closely mimic the optimal performance. Feed-forward augmentation proves particularly efficient at rejecting constant disturbances, while augmentation with integral control is necessary to counter periodic disturbances, where the augmentations are also optimized in the linear-quadratic Gaussian procedures, yet can be closely mimicked by the proposed "rule of thumb" technique.

Keywords: actuator constraints; kinematics; dynamics; intelligent control; automation systems; submersible vehicles; obstacle avoidance; ocean research; guidance, navigation and control; approximated optimal control

1. Introduction

The Naval Postgraduate School's consortium for robotics and unmanned systems education and research (CRUSER) uses three autonomous underwater vehicles, the *Remus*, *Aries* [1], and *Phoenix* [2] vehicles to enhance education and research. The oldest vehicle, *Phoenix* [3] is used in this study to investigate integrated methodologies [4] for vehicle guidance, navigation, and control through a field of obstacles amidst unknown ocean currents that can be approximated by steady state, fixed disturbance ocean velocities, and can also be represented by harmonically oscillating velocities. This integrated approach is a natural extension of the recent innovations. The *Phoenix* vehicle's nominal mathematical modeling was articulated in the 1988 article [5] using surge motion to perform system identification. Recent innovations [6–10] have extended and improved the nominal system identification resulting in high-confidence mathematical modeling in computer simulations. Such simulations permitted Wu et al. [11] to redesign the L1 adaptive control architecture for pitch-control with anti-windup compensation based on solutions to the Riccati equation to guarantee robust and fast adaption of the underwater vehicle with input saturation and coupling disturbances and the approach was applied to the pitch channel alone. Stability was emphasized in the single-channel approach to emphasize dynamic nonlinearities and measurement errors. The Riccati equation is also utilized in this research and proves effective when applied to all six degrees of freedom per [4], where the approach is applied to instances of disturbances that are constant with simultaneous harmonic disturbances simulating unknown ocean currents and waves. In addition to these recent achievements in control, improvements have also been made to guidance and navigation. In recent years, Bo He et al. [12] demonstrated, in simulations and open water experiments, the ability to overcome weak data links and sparse navigation data using a technique called extended information filter (EIF) applied to simultaneous localization and mapping (i.e., "SLAM") that proved computationally easier to implement than the traditional extended Kalman filter (EKF) SLAM. Low computational cost is emphasized here to keep the vehicle size low, but also to exaggerate the laudable goal of achieving optimal or near optimal results with methods that are simple. Such is an overt goal of the new research presented here.

Just last year, Yan et al. [13] integrated the navigation system using a modified fuzzy adaptive Kalman filter (MFAKF) to combine traditional strap-down inertial navigation with OCTANS and Doppler velocity log (DVL) to navigate the challenging polar regions where rapidly converging earth meridians and challenging ocean environments filled with submersed obstacles. This benchmark achievement requires the research here to utilize similar challenging ocean conditions, and provide the motivation for selection of simultaneous steady-state ocean currents together with sinusoidal varying unknown wave conditions amidst an ocean filled with obstacles (where here the non-polar ocean is used, so mines are added to fulfill the role of malignant submersed obstacles). Furthermore, simplified waypoint guidance is derived, based on the onboard-calculated distance from the vehicle to a submerged obstacle. The simplified waypoint guidance is proven effective, and should be considered in situations where onboard operation of a modified fuzzy adaptive Kalman filter proves to be computationally prohibitive. The distance to an underwater obstacle was measured by Wang et al. [14] with a novel method: measuring extremely low frequency (ELF) emissions with onboard inductive sensors. Such emissions are produced by ship hulls with relatively pronounced amplitudes compared to small subsurface obstacles, but the harmonic line spectra and fundamental signal frequency relate directly to the closing speed of approach to the obstacle. Experiments proved that even such small signals were detectable at long range with high sensitivity and low-noise sensors of the current state of the art, thus closing the distance to obstacles may now be presumed to be known passively,

permitting the simplified waypoint guidance proposed in this manuscript. Particularly after ELF queuing, position, orientation, and velocity of obstacles may be monitored optically, as developed by Eren et al. [15], and these states may be used as feedback signals together with the waypoint guidance (desired trajectory) permitting augmentation with linear quadratic Gaussian techniques, as performed in this manuscript where full-order state observers are together optimized with attitude controller gains, followed by demonstration that reduced-order observers may also be optimized allowing vehicle operators to compensate for individually failed or degraded sensors, or instances where optimally-estimated signals are superior to sensor signals in individual or multiple channels.

Integrating these latest technological developments was demonstrated last year by Wei et al. [16], who integrated the Doppler velocity methods for obstacle monitoring into a dynamic obstacle avoidance scheme for collision avoidance. Following data fusion, a collision risk assessment model is used to avoid collisions, and claims to be effective in unknown dynamic environments, although the experiments did not go so far as to stipulate near-constant ocean currents in addition to harmonic wave actions. These challenging dynamic environments are addressed in this manuscript as a natural extension of the current state of the art.

Autonomous vehicle angular momentum control of rotational mechanics may be achieved using control moment gyroscopes, one potential momentum exchange actuator with a long, historic legacy of actuating space vehicles, where mathematical singularities have just recently been overcome [17–23], permitting the use of the actuator for underwater vehicles as recently achieved by Thorton et al. [24,25], including combined attitude and energy storage control. These developments suffice to reveal that attitude control is not controversial and, thus, the remainder of this manuscript focuses on guidance and navigation with a residual necessity to implement nominal, effective pitch and yaw control.

2. Materials and Methods

Assuming the availability of the recent technologies cited in the Introduction, this section describes the proposed methods to use these technologies to guide a submersed vehicle along a preplanned path through a field of randomly-placed obstacles. The constituent technologies are investigated through this section of the manuscript, and then combined in a fully-assembled system demonstration in Section 3 (Results), where the figure of merit used to assess the efficacy of the proposed methods is the maintenance of the miss distance from submersible objects in ocean currents.

Submersible vehicles require control systems to guide the vehicle around obstacles that can present dangers to vehicle health and safety in the presence of ocean currents. The challenge addressed here is to navigate one of the two Naval Postgraduate School's submersible vehicle (Figures 1 and 2) through a simulated minefield whose dimensions are 200 m \times 5100 m in the presence of 0.5 m/s ocean currents. The field will contain at least 30 mines placed at locations using a random number generator. The resulting controller structure has an inner-outer loop structure, and several technologies will be described including pole-placement designs, linear-optimal (quadratic) Gaussian techniques, full- and partial-order observers for online disturbance identification for ocean currents (both constant lateral underwater ocean currents and also sinusoidal varying currents), tracking systems and feed-forward control designed to counter open ocean currents, in addition to integral control. The outer loop controller uses line-of-sight (LOS) guidance to provide a heading command to the inner loop. The inner loop controller uses output heading feedback to track heading commands. The vehicle is simulated to traverse a minefield and successfully travels no closer than 5 m from any mine and arrives within from the commanded destination autonomously; while this overall system design requirement drives subsystem requirements for trajectory tracking.

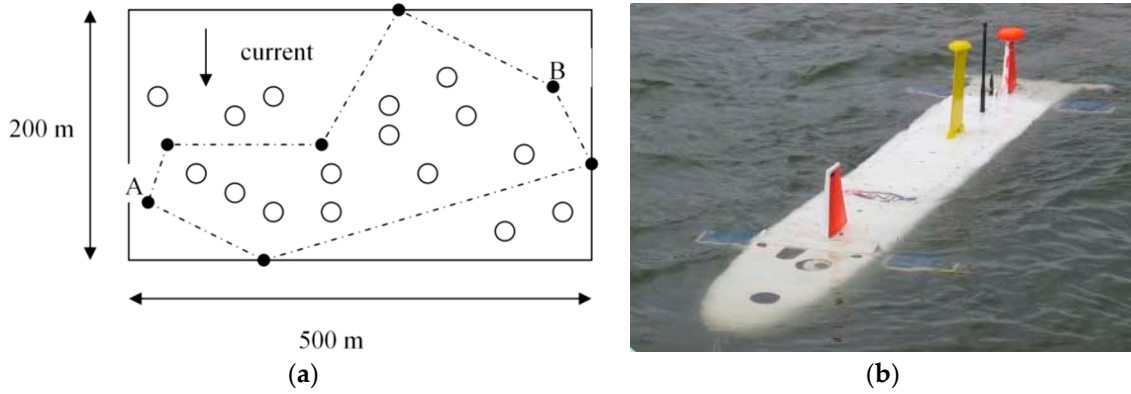


Figure 1. Submersible vehicle sample and notional minefield [1]. (a) Field of randomly-placed submersed mines to be avoided by the autonomous vehicle; and (b) *Aries* submersible in open ocean (illustrative sample is not simulated; the Figure 2 *Phoenix* vehicle is simulated).

2.1. System Dynamics

The equations of motion used to simulate the dynamic behavior of the autonomous submersible vehicle in a horizontal plane are listed in Equations (1)–(4). All variables in these equations are assumed to be in nondimensional form with respect to the vehicle length (7.3 feet) and constant forward speed (~3 ft/s). The vehicle weighs 435 lbs and is neutrally buoyant. Time is non-dimensionalized such that 1 s represents the time it takes to travel one vehicle length.

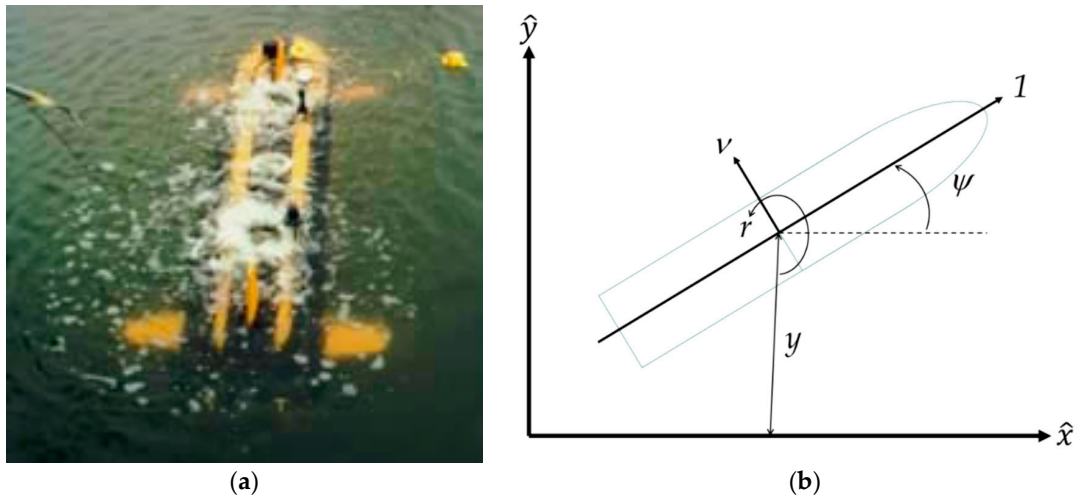


Figure 2. Vehicle geometry and reference axes. (a) *Phoenix* in open ocean [1]. The experimentally-determined dynamic model for this vehicle is listed in Equations (1)–(6) and forms the basis for the simulations in this manuscript; and (b) vehicle geometry and reference axis.

$$(m - Y_{\dot{v}})\dot{v} - (Y_{\dot{r}} - mx_G)\dot{r} = Y_r v + (Y_r - m)r + Y_{\delta_s} \delta_s + Y_{\delta_b} \delta_b \tag{1}$$

$$(mx_G - N_{\dot{v}})\dot{v} - (N_{\dot{r}} - I_z)\dot{r} = N_v v + (N_r - mx_G)r + N_{\delta_s} \delta_s + N_{\delta_b} \delta_b \tag{2}$$

$$\dot{\psi} = r \tag{3}$$

$$\dot{y} = \sin\psi + v\cos\psi \tag{4}$$

In addition to the following dependent equation:

$$\dot{x} = \cos\psi - v\sin\psi \tag{5}$$

	where the variables are	and the constants are	$Y_{\delta_s} = 0.01241$
v	Lateral (sway) velocity	$m = 0.0358$	$Y_{\delta_b} = 0.01241$
r	Turning rate (yaw)	$I_z = 0.0022$	$N_r = -0.00047$
ψ	Heading angle (degrees)	$x_G = 0.0014$	$N_v = -0.00178$
y	Lateral deviation (cross-track error)	$Y_r = -0.00178$	$N_r = -0.00390$
δ_s	Stern rudder deflection	$Y_v = -0.03430$	$N_v = -0.00769$
δ_b	Bow rudder deflection	$Y_r = 0.01187$	$N_{\delta_s} = -0.0047$
		$Y_v = -0.10700$	$N_{\delta_b} = 0.0035$

The constant definitions in the mass m , mass moment of inertia with respect to a vertical axis that passes through the vehicle’s geometric center (amidships) I_z , position of the vehicle’s center of gravity (measured positive forward of amidships) x_G , with the remaining terms referred to as the hydrodynamic coefficients. These constants are all presented in non-dimensional form.

Defining the state vector $\{x\} \equiv \{v \ r \ \psi \ y\}^T$ and the control $\{u\} \equiv \{\delta_s \ \delta_b\}^T$ and assuming small angles, the dynamics expressed in Equations (1)–(4) may be expressed in state space form as $\{\dot{x}\} = [A]\{x\} + [B]\{u\}$ where:

$$[A] = \begin{bmatrix} -1.4776 & -0.3083 & 0 & 0 \\ -1.8673 & -1.2682 & 0 & 0 \\ 0 & 1 & 0 & 0 \\ 1 & 0 & 1 & 0 \end{bmatrix} \quad [B] = \begin{bmatrix} 0.2271 & 0.1454 \\ -1.9159 & 1.2112 \\ 0 & 0 \\ 0 & 0 \end{bmatrix} \quad (6)$$

The system may also be expressed in a transfer function ratio of outputs divided by inputs in Laplace form using Equation (7) where the observer matrix $[C]$ is merely a proper identity matrix to this point of the manuscript. Equation (7) yields two transfer function relationships between each of the two possible rudder inputs as seen in Equations (8) and (9). Notice that both transfer functions have poles and zeros at the origin, while pole-zero cancellation is possible in the case of the stern rudder. On the other hand, even after pole-zero cancellation in the bow rudder Equation (9), there remains an open loop pole at the origin that must be dealt with during the control design, since it represents a potentially unstable element (at the very least, in the instance where the estimated constants are exactly correct, and these equations of motion exactly describe the system, an oscillatory element exists that will not decay). Nonetheless, the dynamics accord to nature. Consider trying to steer a row-boat using the rear rudder: it is much more stable than trying to steer the rowboat using a rudder in the front. This analogy applies to the submersible vehicle and is verified in these results.

$$G(S) = [C](s[I] - [A])^{-1}[B] \quad (7)$$

$$G(S)|_{\delta_s} \equiv \frac{Y(s)}{\delta_s(s)} = \frac{0.2271s^3 + 0.875s^2}{s^4 + 2.746s^3 + 1.298s^2} = \frac{s^2(0.2271s + 0.875)}{s^2(s^2 + 2.746s + 1.298)} \quad (8)$$

$$G(S)|_{\delta_b} \equiv \frac{Y(s)}{\delta_b(s)} = \frac{1.211s^2 + 1.518s}{s^4 + 2.746s^3 + 1.298s^2} = \frac{s(1.211s + 1.518)}{s^2(s^2 + 2.746s + 1.298)} \quad (9)$$

In Figure 3, the uncontrolled system is analyzed by merely performing a circular turn with each (and then both) rudders. The bow and stern rudders alone are each compared to the combined use of both bow and stern rudders. The bow rudder was deflected +15 degrees for about 21 s, while the stern rudder was deflected for –15 degrees for about 11 s. When both rudders were deflected the maneuver was completed in roughly 8 s. Two initial conditions for the sway velocity were investigated ($v(0) = 0$ and then $v(0) = \sqrt{8}$). In all cases, the bow rudder alone performed the poorest, with the stern rudder alone performing the turn in a smaller radius and shorter time. Furthermore, the combined use of both rudders resulting in tightest maneuver.

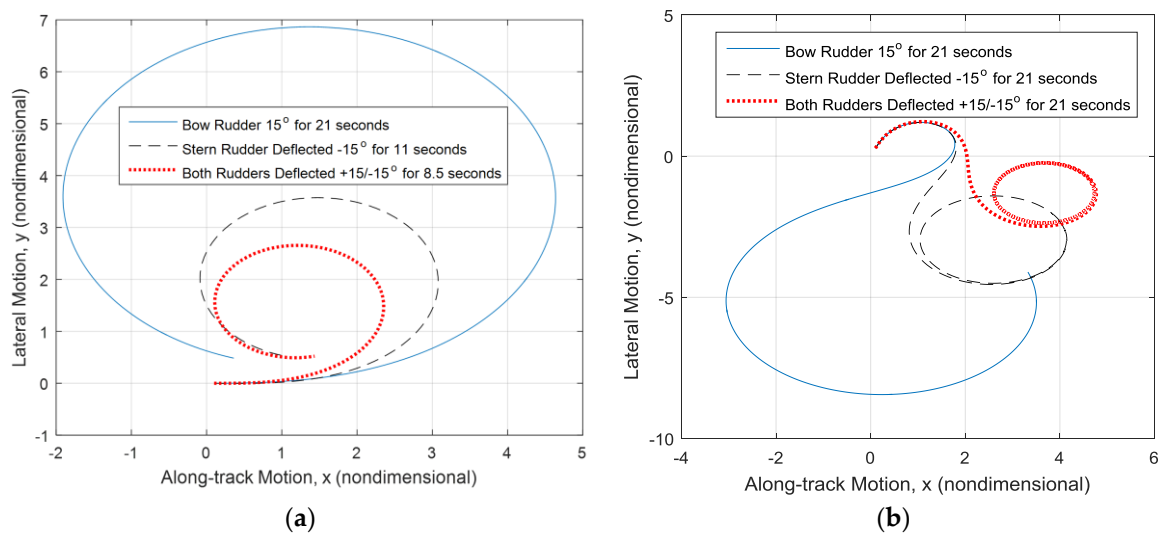


Figure 3. Analysis of uncontrolled system: comparison of rudder performance. (a) Counter-clockwise turn, $v(0) = 0$; and (b) initial sway velocity $v(0) = \sqrt{8}$.

Two simulation methodologies were used to investigate sensitivities to integration method. MATLAB was used with Euler integration, while SIMULINK was used with Runge-Kutte integration with identical timesteps, $\Delta t = 0.1$ s. Both software packages are manufactured and supplied by Mathworks®, Natick, Massachusetts, USA. The results were nearly negligible and are displayed in Table 1, from which insensitivity to the integration approach is established.

Table 1. Comparison of simulation integration methodologies.

Rudder Deflected	Euler: x-Distance ¹	Runge-Kutte: x-Distance ¹	Euler: y-Distance ¹	Runge-Kutte: y-Distance ¹
Bow	6.5471	6.5469	6.8647	6.8646
Stern	3.1665	3.1665	3.5768	3.5768
Both	2.4546	2.4546	2.6567	2.6567

¹ Distances calculated to traverse one circular path.

2.2. Control Law Design

In the system analysis, the optimal rudder implementation scheme was determined to be the application of both rudders, where the rudders were slaved to the same maneuver angle magnitude with the opposite sign, i.e., a “scissored-pair”, per Equation (10). In the case where only variable y is to be measured, the new state space formulation of the system equation components are in Equation (11). Under the assumption of rudders constrained to behave as a scissored-pair the transfer function from rudder input to output y is given by Equation (12) whose poles and zeros are listed in Equation (13), with Equation (14) revealing the system’s eigenvalues, noting the values are identical to the location of the poles in accordance with theory. The controllability and observability matrices ([CO] and [OB], respectively) are listed in Equation (15) (whose matrix product [OC] is in Equation (16)) verifying these system equations are both controllable and observable, since these matrices are full-rank, while the determinant of the controllability matrix is 63.1778, a large value with a small value of the matrix condition number, 13.4513. The non-zero determinant of the controllability matrix proves controllability, but to see how close the system is to being uncontrollable, the matrix condition number proves more useful. These two figures of merit indicate the system equations are highly controllable and, accordingly, this manuscript will investigate and compare several options for navigation control: pole placement, linear quadratic optimal control, linear quadratic Gaussian, and time optimal control. The same holds true for observability and, thus, linear quadratic Gaussian. The matrix product [OC] is the same for every definition of state variables for the given system.

A change in system parameters results in disparate system equation coefficients in Equations (1)–(5) which may be expressed in state space or transfer-function formulations and correlated modifications to Equations (6), (8), and (9). Nonetheless, these equations form the basis for finding linear-quadratic Gaussian optimal solutions or the simpler rule-of-thumb procedure driven by system time-constant. Since the process for finding the optimal solutions is inherently more challenging than simple control calculations using the time-constant, the rule of thumb technique is generically superior in regards to computational overhead, regardless of system parameters chosen.

$$\delta_b = -\delta_s \tag{10}$$

$$[A] = \begin{bmatrix} -1.4776 & -0.3083 & 0 & 0 \\ -1.8673 & -1.2682 & 0 & 0 \\ 0 & 1 & 0 & 0 \\ 1 & 0 & 1 & 0 \end{bmatrix} [B] = \begin{bmatrix} 0.0816 \\ -3.1271 \\ 0 \\ 0 \end{bmatrix} [C] = [0 \ 0 \ 0 \ 1] [D] = [0] \tag{11}$$

$$G(S)|_\delta \equiv \frac{Y(s)}{\delta(s)} = \frac{0.08164s^2 - 2.06s - 4.773}{s^4 + 2.746s^3 + 1.298s^2} \tag{12}$$

$$\text{poles at : } s = 0, 0, -0.6070, -2.1388; \text{ zeros at : } s = -6.1279 \times 10^{13}, \text{ near } -0, \text{ near } -0 \tag{13}$$

$$\text{eig}(A) = \lambda = 0, 0, -0.6070, -2.1388 \tag{14}$$

$$[CO] = \begin{bmatrix} 0.0816 & 0.8433 & -2.4216 & 5.5544 \\ -3.1271 & 3.8132 & -6.4105 & 12.6514 \\ 0 & -3.1271 & 3.8132 & -6.4105 \\ 0 & 0.0816 & -2.2838 & 1.3916 \end{bmatrix} [OB] = \begin{bmatrix} 0 & 0 & 0 & 1 \\ 1 & 0 & 1 & 0 \\ -1.4776 & 0.6917 & 0 & 0 \\ 0.8917 & -0.4217 & 0 & 0 \end{bmatrix} \tag{15}$$

$$[OC] = \begin{bmatrix} 0 & 0.0816 & -2.838 & 1.3916 \\ 0.0816 & -2.2838 & 1.3916 & -0.8561 \\ -2.2838 & 1.3916 & -0.8561 & 0.5441 \\ 1.3916 & -0.8561 & 0.5441 & -0.3825 \end{bmatrix} \tag{16}$$

Diagonalizing the original system $[A]$ matrix, the spectral decomposition $[T][\Lambda] = [A][T] \rightarrow [\Lambda] = [T]^{-1}[A][T]$ in Equation (17) may be used to verify a diagonal matrix of eigenvalues $[\Lambda]$, and then write the system of equations in *normal-coordinate form* $\{x'\} = [A']\{x'\} + [B'][u]; \{y'\} = [C']\{x'\}$ using the following transformation: $[A'] = [\Lambda] = [T]^{-1}[A][T]$, $[B'] = [T]^{-1}[B]$, and $[C'] = [C][T]$ whose results are in Equation (18):

$$[\Lambda] = \underbrace{\begin{bmatrix} 0.4663 & -0.1074 & 0 & 0 \\ 1 & 0.3033 & 0 & 0 \\ -0.4676 & -0.4996 & 0 & 0 \\ 0.0006 & 1 & 1 & -1 \end{bmatrix}}_{T^{-1}} \underbrace{\begin{bmatrix} -1.4776 & -0.3083 & 0 & 0 \\ -1.8673 & -1.2682 & 0 & 0 \\ 0 & 1 & 0 & 0 \\ 1 & 0 & 1 & 0 \end{bmatrix}}_A \underbrace{\begin{bmatrix} 0.4663 & -0.1074 & 0 & 0 \\ 1 & 0.3033 & 0 & 0 \\ -0.4676 & -0.4996 & 0 & 0 \\ 0.0006 & 1 & 1 & -1 \end{bmatrix}}_T \tag{17}$$

$$[A'] = \begin{bmatrix} -2.1388 & 0 & 0 & 0 \\ 0 & -0.6070 & 0 & 0 \\ 0 & 0 & 0 & 0 \\ 0 & 0 & 0 & 0 \end{bmatrix}, [B'] = \begin{bmatrix} -1.2502028 \\ -6.1888806 \\ -8.4625 \times 10^7 \\ -8.4625 \times 10^7 \end{bmatrix}, [C'] = \{ 0.0006 \ 1 \ 1 \ -1 \} \tag{18}$$

$$\{u\}_{baseline} = \{\delta\} = -K_v v - K_r r - K_\psi \psi - K_y y \tag{19}$$

For the pole placement proportional-derivative (PD) controller articulated in Equation (19), the poles are set to have roughly the same time constant, while avoiding exactly coincident poles. Gains are iterated for various time constants as displayed in Figure 4, but the following rule of thumb is asserted as well to quickly achieve performance that closely mimics the performance of linear-quadratic optimal (LQR) gains where the control effort and tracking error are equally weighted in the cost function of the optimization. Since the rule-of-thumb method uses the assumed system

model for computation of the control, it is particularly generic. References [7,9,10] each contain methods for online system parameter identification (with a motivation of use in the finding the control signal), permitting the rule of thumb's generic applicability, since it is expressed in terms of the system parameters.

RULE OF THUMB: Select unity time-constant t_c to roughly locate closed-loop poles per Equation (20). Then place other poles at slightly different locations (e.g., $s_p = s_1 \pm 0.01 \forall p$)

$$Pole : s_1 = \frac{1}{t_c} \tag{20}$$

The gains achieved using the rule of thumb $K_{R.O.T.} = \{0.5070 \ -0.3687 \ -0.7157 \ -0.1972\}$ (see Table 2) have quite different values compared to the gains calculated through the matrix Riccati equation in the linear-quadratic optimization $K_{LQR} = \{-0.0939 \ -1.2043 \ -2.2138 \ -1\}$, but, nonetheless, the resulting behaviors are indeed very similar.

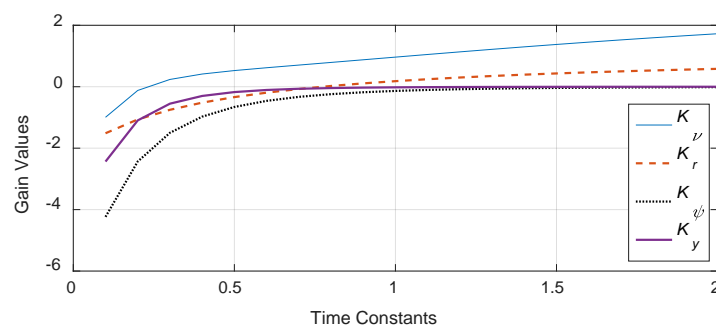


Figure 4. Gain values for each state iterated for various time constants.

Next, the initial feedback control design was evaluated in simulations where the ship is initially located off the desired track by one ship's length port side with zero heading, and rudder deflection was limited to 0.4 radians (~23 degrees). Next, another simulation was performed to test an initial heading angle of 30 degrees starboard where the initial $y(0) = 0$. The results are displayed in Figure 5a,b, respectively. All state variations were plotted in Figure 4, highlighting the fact that y converges to zero along with the other states. Furthermore, the results of rudder-limited simulations are displayed in Figure 6 for both scenarios, while the comparison of *rule of thumb* to LQR is shown in Figure 7.

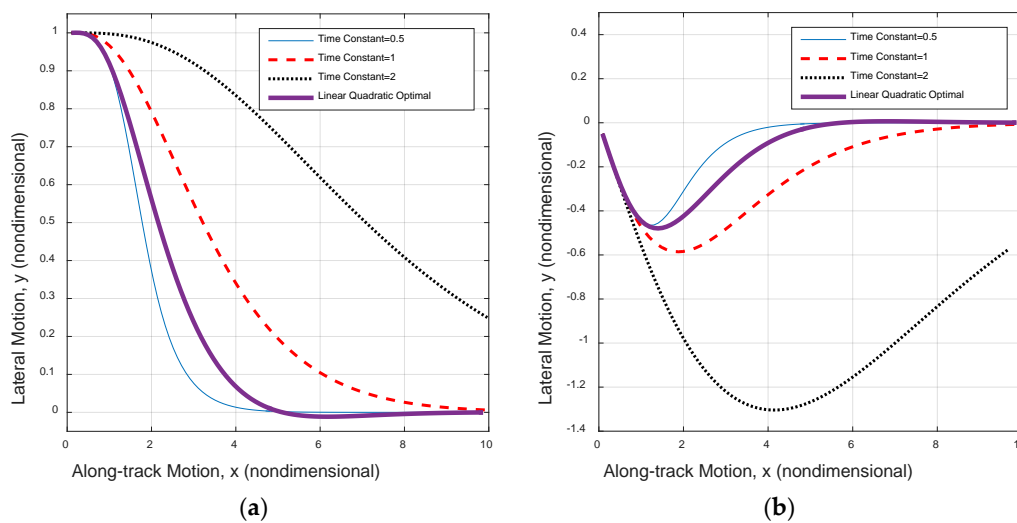


Figure 5. Simulations testing the initial baseline feedback controller in two scenarios. (a) Initially one ship's length port side; and (b) initial heading 30° starboard.

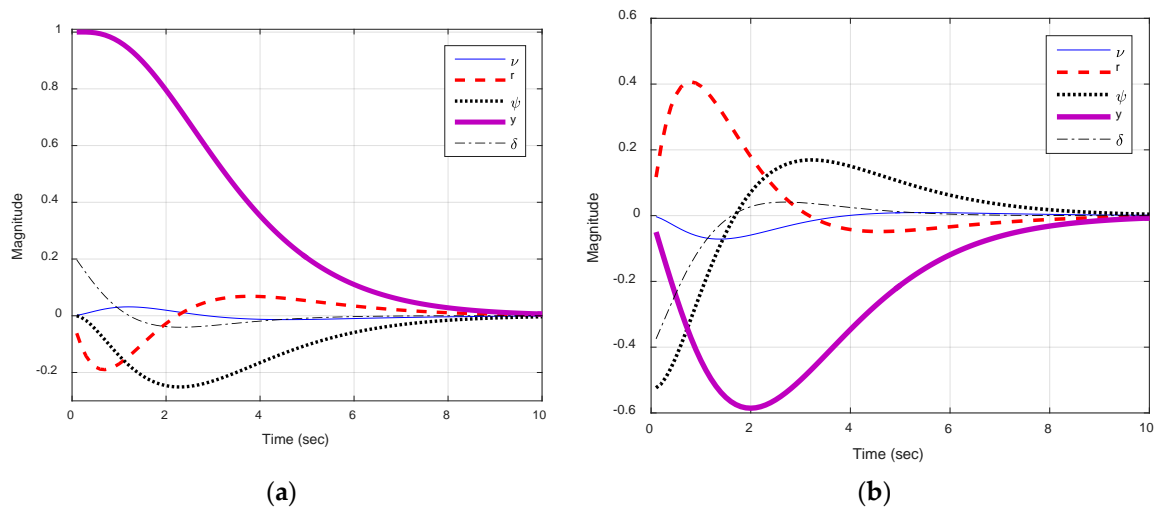


Figure 6. State variations for both scenarios simulated using pole-placement gains via *rule of thumb*. (a) Initially one ship's length port side; and (b) initial heading 30° starboard.

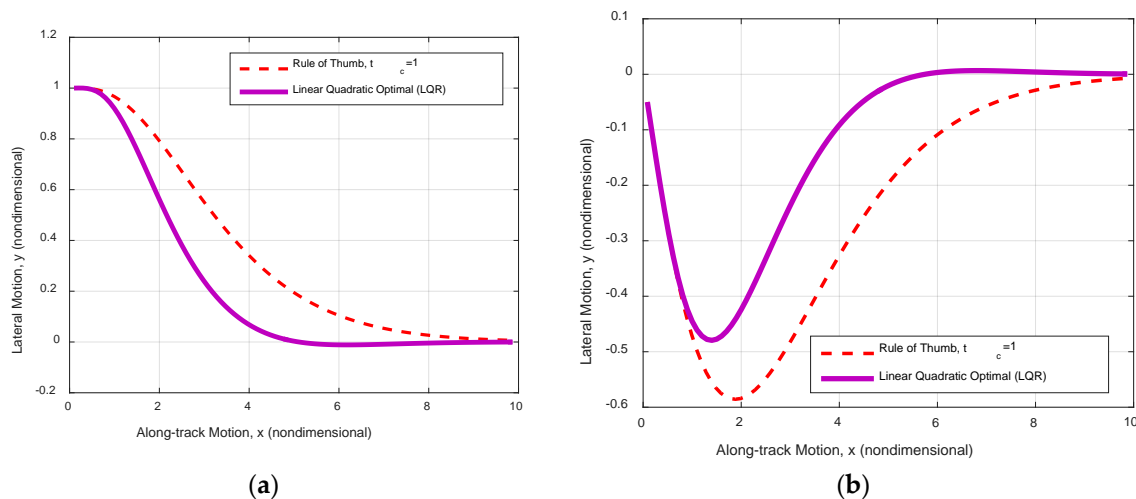


Figure 7. Rudder-limited trajectory track using pole-placement gains via *rule of thumb* and LQR. (a) Initially one ship's length port side; and (b) initial heading 30° starboard.

Table 2. Gains for various time constants and also solution to linear quadratic optimization.

Time Constant	K_ν	K_r	K_ψ	K_y
0.5	-1.5135	-1.7005	-5.1508	-3.22524
1	0.5070	-0.3687	-0.7157	-0.1972
2	1.1248	0.2870	-0.0906	-0.0116
LQR	-0.0939	-1.2043	-2.2138	-1

¹ Reminder: state definition $\{x\} \equiv \{ \nu \ r \ \psi \ y \}^T$.

2.3. Observer Design

To design a state observer, the system must be observable [4], verifiable through examination of the observability matrix $[OB]$ per Equation (21), where for example $[C] = [\nu \ r \ \psi \ y] = [0 \ 1 \ 1 \ 1]$, while several such examples will be iterated in this investigation. The condition of the observability matrix reveals the degree of observability, and it is defined by the ratio of maximum to minimal singular values:

$$[OB] = \begin{bmatrix} C \\ CA \\ CA^2 \\ \vdots \\ CA^{n-1} \end{bmatrix} \tag{21}$$

2.3.1. Full-Order Observer Design

$$\{\dot{\hat{x}}\} = [A]\{\hat{x}\} + [B][u] + [L](\{y\} - [C]\{\hat{x}\}) \tag{22}$$

$$\{\dot{x}\} - \{\dot{\hat{x}}\} = [A]\{x\} - [A]\{\hat{x}\} - [L]([C]\{x\} - [C]\{\hat{x}\}) \tag{23}$$

$$\{\dot{e}\} \equiv \{\dot{x}\} - \{\dot{\hat{x}}\} = ([A] - [L][C])(\{x\} - \{\hat{x}\}) \tag{24}$$

$$\{\dot{e}\} = ([A] - [L][C])\{e\} \tag{25}$$

Assuming that only ν measurements are available, a mathematical model of the estimated system is shown in Equation (22) with a full-order observer design using the observer error Equation (23) leading to the error vector in Equation (24) allowing the re-expression of Equation (22) as Equation (25), where the dynamic behavior of the error vector is determined by the eigenvalues of matrix $[A] - [L][C]$, where $[L]$ gains of the observer may be chosen as desired for systems that prove observable, such that the error vector will converge to zero for any stable $[A] - [K_e][C]$. In the following paragraphs, $[L]$ is designed by solving the matrix Riccati equation leading to linear quadratic optimal gains, and also by solving the *rule of thumb* relationship between gains and time constant as done for the controller gains resulting in Table 3.

Table 3. Full-order observer gains designed by *rule of thumb* for various time constants as multiple of controller time constant, t_c .

Multiple of the Controller Time Constant Used for the Observer	Observer Gain Matrix
$\frac{1}{2}t_c$	$\{ -0.7464 \quad 1.8077 \quad 8.8270 \quad 5.1942 \}^T$
$10t_c$	$10^3 * \{ -1.5909 \quad -3.4121 \quad 1.5953 \quad -0.0020 \}^T$

¹ Reminder: $\frac{1}{2}t_c$ is used in subsequent simulations.

Figure 8 displays the results of simulations revealing the accuracy of state estimation when $[L]$ is calculated by the *rule of thumb*, where the time constant is chosen to be half ($t_c = 1/2$) the time constant of the controller ($t_c = 1$), and the simulation is initialized with the heading angle 30 degrees off, while Figure 9 displays the simulation initialized at the one boat-length starboard position.

2.3.2. Reduced-Order Observer Design

Assuming that some measurements are available from sensors, this paragraph describes the possible iterations and reveals states that are relatively more important to measure with sensors. Four possible output matrices are used to investigate observability. Four options for output matrices $[C]_i$ for $i = 1, \dots, 4$ result in four reduced-order observers $[OB]_i$ for $i = 1, \dots, 4$ are detailed in Equations (26)–(29). The output matrix $[C]_1$ produces an observability matrix $[OB]_1$ with rank = 4 (observable) and determinant not nearly equal to zero. The output matrix $[C]_2$ produces an observability matrix $[OB]_2$ with rank = 4 (observable) and determinant not nearly equal to zero. The output matrix $[C]_3$ produces an observability matrix $[OB]_3$ with rank = 4 (observable) and determinant nearly equal to zero. The matrix condition number is very high indicating the system is barely observable. The output matrix $[C]_4$ produces an observability matrix $[OB]_4$ with rank = 3 (not observable) and determinant equal to zero with a matrix condition number equal to

infinity. This means if all other states are measured by sensors, it is not possible to use an observer (even an optimal observer) to determine lateral deviation (cross-track error), y . It is a key state to measure with sensors. The sensor combinations that include y are observable. Using every other sensor, (except y) results in a system that is not observable. Furthermore, measuring y alone results in a barely observable system.

$$[C]_1 = \begin{Bmatrix} v \\ r \\ \psi \\ y \end{Bmatrix} = \begin{Bmatrix} 0 \\ 1 \\ 1 \\ 1 \end{Bmatrix} \rightarrow [OB]_1 = \begin{bmatrix} C \\ CA \\ CA^2 \\ \vdots \\ CA^{n-1} \end{bmatrix} = \begin{bmatrix} 0 & 1 & 1 & 1 \\ -0.8673 & -0.2682 & 1 & 0 \\ 1.7823 & 1.6074 & 0 & 0 \\ -5.6352 & -2.5879 & 0 & 0 \end{bmatrix} \quad (26)$$

$$[C]_2 = \begin{Bmatrix} v \\ r \\ \psi \\ y \end{Bmatrix} = \begin{Bmatrix} 0 \\ 1 \\ 0 \\ 1 \end{Bmatrix} \rightarrow [OB]_2 = \begin{bmatrix} C \\ CA \\ CA^2 \\ \vdots \\ CA^{n-1} \end{bmatrix} = \begin{bmatrix} 0 & 1 & 0 & 1 \\ -0.8673 & -1.2682 & 1 & 0 \\ 3.6496 & 2.8756 & 0 & 0 \\ -10.7624 & -4.7717 & 0 & 0 \end{bmatrix} \quad (27)$$

$$[C]_2 = \begin{Bmatrix} v \\ r \\ \psi \\ y \end{Bmatrix} = \begin{Bmatrix} 0 \\ 0 \\ 0 \\ 1 \end{Bmatrix} \rightarrow [OB]_3 = \begin{bmatrix} C \\ CA \\ CA^2 \\ \vdots \\ CA^{n-1} \end{bmatrix} = \begin{bmatrix} 0 & 0 & 0 & 1 \\ 1 & 0 & 1 & 0 \\ -1.4776 & 0.6917 & 0 & 0 \\ 0.8917 & -0.4217 & 0 & 0 \end{bmatrix} \quad (28)$$

$$[C]_2 = \begin{Bmatrix} v \\ r \\ \psi \\ y \end{Bmatrix} = \begin{Bmatrix} 1 \\ 1 \\ 1 \\ 0 \end{Bmatrix} \rightarrow [OB]_4 = \begin{bmatrix} C \\ CA \\ CA^2 \\ \vdots \\ CA^{n-1} \end{bmatrix} = \begin{bmatrix} 1 & 1 & 1 & 0 \\ -3.3450 & -0.5764 & 1 & 0 \\ 6.90190 & 1.7621 & 0 & 0 \\ -12.1843 & -4.0900 & 0 & 0 \end{bmatrix} \quad (29)$$

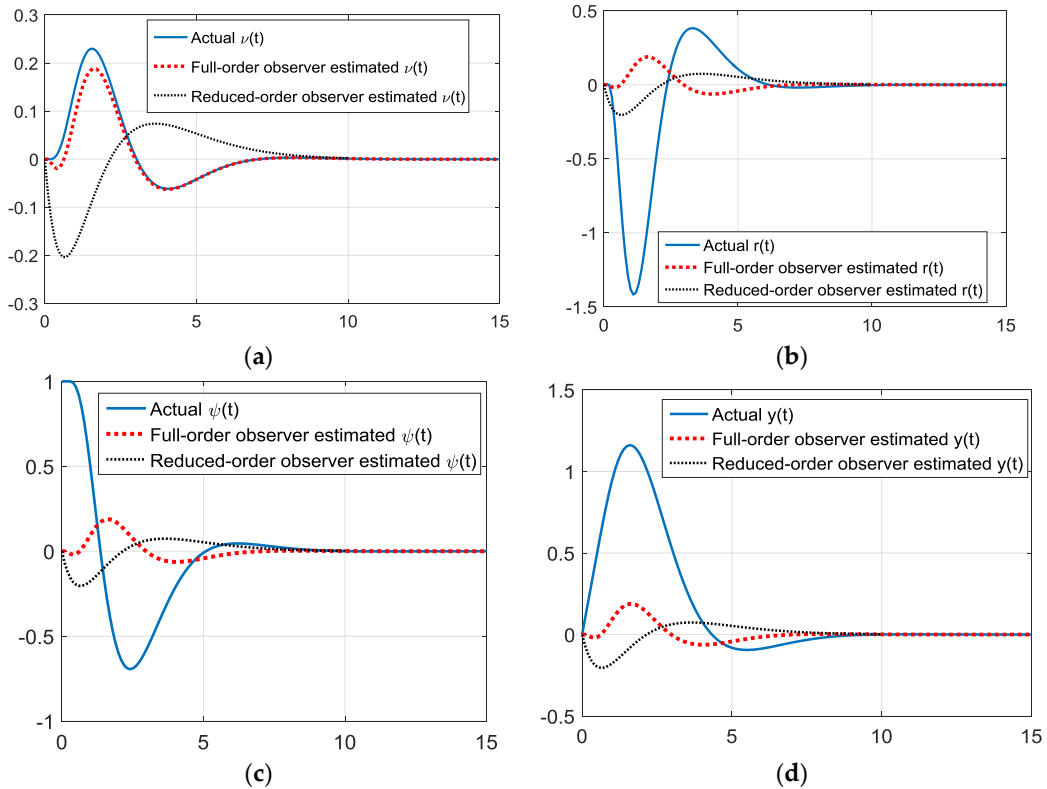


Figure 8. Simulations starting 30 degrees off heading with gains via *rule of thumb* state observer gains. (a) True and estimated sway velocity, $v(t)$; (b) true and estimated turning rate, $r(t)$; (c) true and estimated heading angle, $\psi(t)$; and (d) true and estimated cross track, $y(t)$.

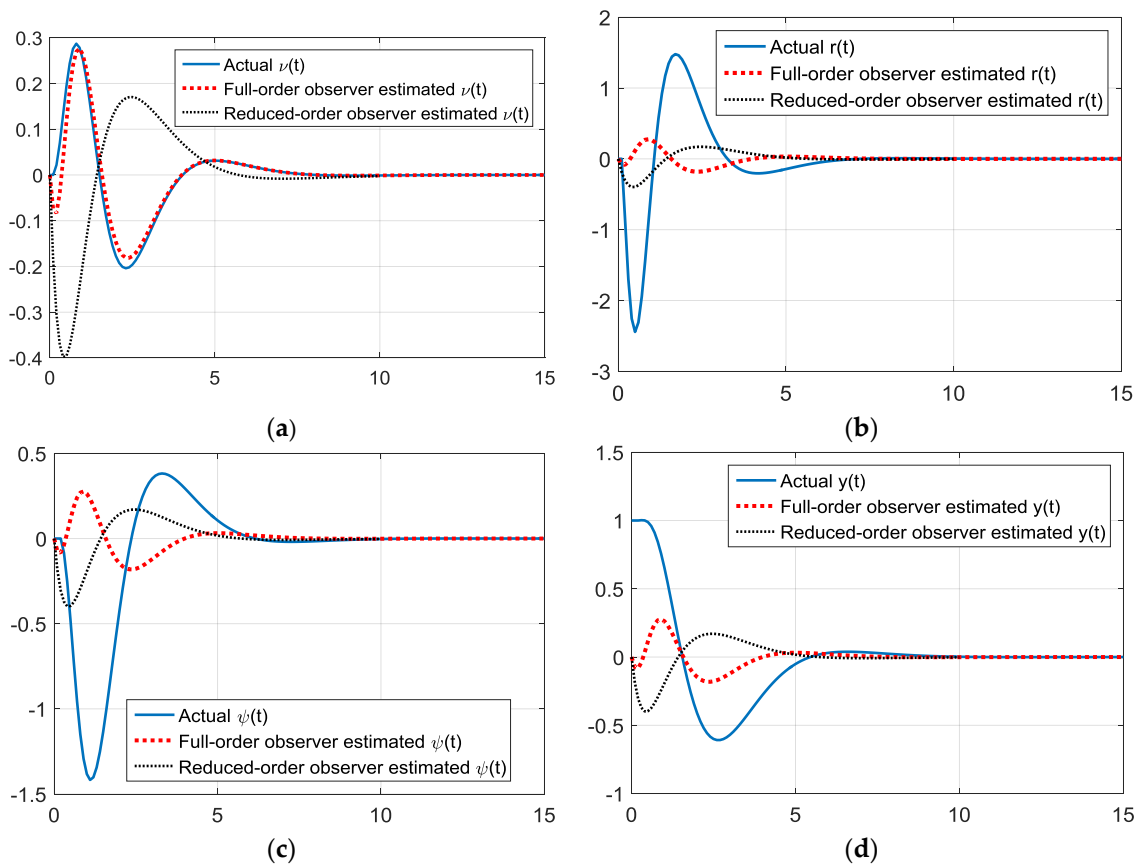


Figure 9. Simulations starting one boat-length starboard with gains via *rule of thumb*. (a) True and estimated sway velocity, $v(t)$; (b) true and estimated turning rate, $r(t)$; (c) true and estimated heading angle, $\psi(t)$; and (d) true and estimated cross track, $y(t)$.

Assuming y is to be measured by a sensor, Table 4 reveals that measuring v in addition to y produces the most observable system, and is recommended for designing reduced-order observers. The drawback is measuring v requires a Doppler sonar, which may not always be available. If all states are measurable except v the resulting reduced-order observer merely estimates v using gains on the measurable states displayed in Table 5. Figure 10 reveals a very good estimation of v when all other states are sensed, and this estimated value of v was fed to the motion controller in addition to the measured states (the poorly estimated states were neglected instead favoring the more-accurate measurements). State convergence to zero is achieved in the instance of state initialization 30 degrees off-heading. Figure 11 displays similar results for the instance of state initialization one boat-length starboard.

Table 4. Observability matrix condition number for options to supplement the y measurement.

Sensors Used to Measure States	Observability Matrix Condition Number ¹
y and v	8.8456
y and r	21.1306
y and ψ	31.2919

¹ Reminder: a high condition number means a less observable system.

Table 5. Reduced-order observer gains designed by *rule of thumb* for various time constants as a multiple of the controller time constant, t_c .

Multiple of the Controller Time Constant Used for Observer	Observer Gain Matrix
$\frac{1}{10}t_c$ ¹	$\begin{Bmatrix} -0.2174 & 0 & 0.1164 \end{Bmatrix}^T$
$2t_c$	$\begin{Bmatrix} 0.4069 & 0 & -0.2179 \end{Bmatrix}^T$
$10t_c$	$\begin{Bmatrix} 0.5941 & 0 & -0.3182 \end{Bmatrix}^T$

¹ Relatively faster $\frac{1}{10}t_c$ is used in subsequent simulations.

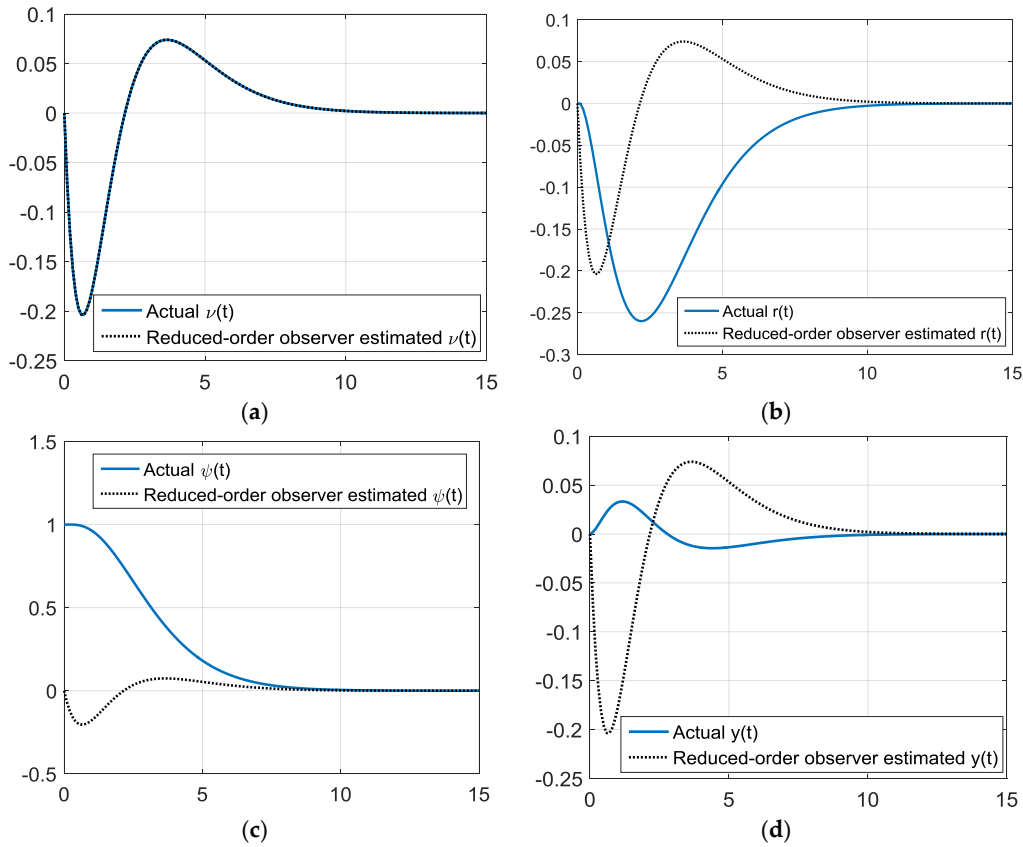


Figure 10. Simulations starting 30 degrees off heading gains via *rule of thumb* reduced-order state observer gains. (a) True and estimated sway velocity, $\nu(t)$ versus time (seconds); (b) true and estimated turning rate, $r(t)$ versus time (seconds); (c) true and estimated heading angle, $\psi(t)$ versus time (seconds); and (d) true and estimated cross track, $y(t)$ versus time (seconds).

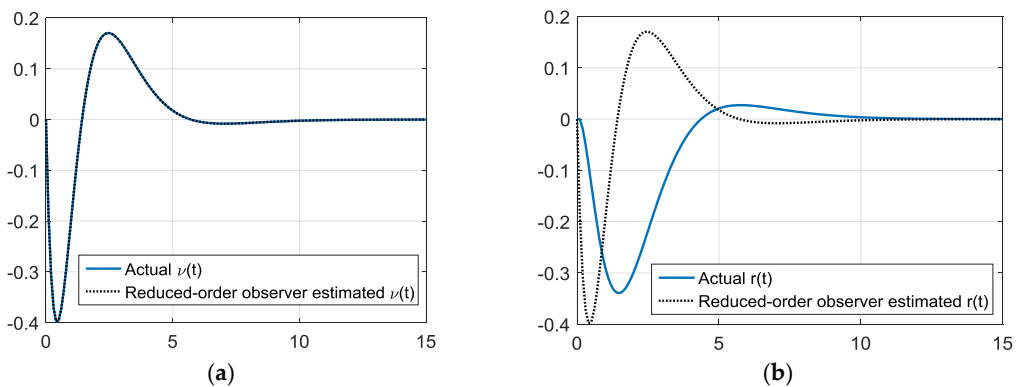


Figure 11. Cont.

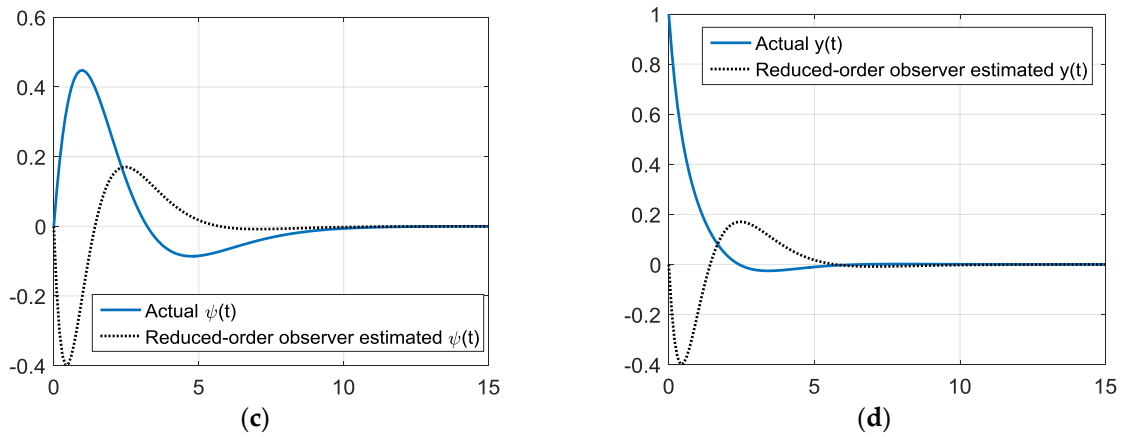


Figure 11. Simulations starting one boat-length starboard with gains via *rule of thumb* reduced-order state observer gains. (a) True and estimated sway velocity, $v(t)$ versus time (seconds); (b) true and estimated turning rate, $r(t)$ versus time (seconds); (c) true and estimated heading angle, $\psi(t)$ versus time (seconds); and (d) true and estimated cross track, $y(t)$ versus time (seconds).

2.3.3. Gain Margin and Phase Margin

Figure 12 compares the loop gains of the system with and without a compensator via the gain margin and phase margin with full-state feedback, while Figure 13 displays the loop gains when output-feedback via observers is used. Each has relative strengths. Full state (theoretical) feedback yields an infinite gain margin, yet a relatively lower phase margin (usually consider more important of the two), while output feedback (real-world) yields a good (but lesser) gain margin with an increased phase margin.

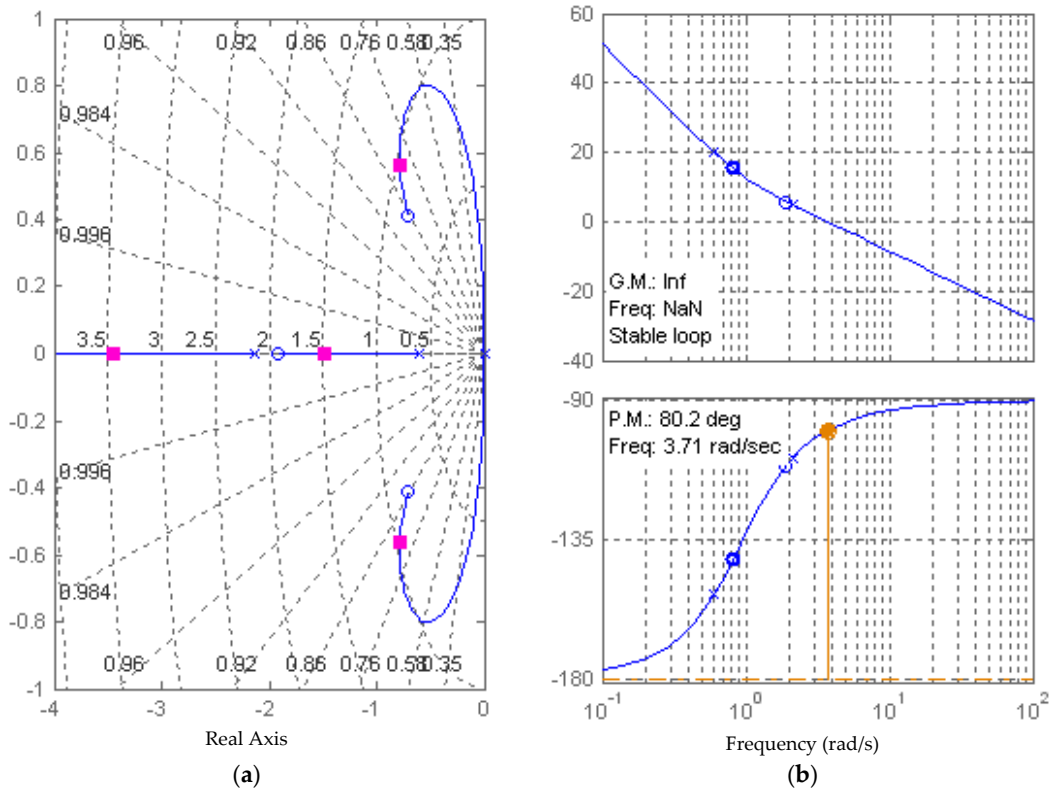


Figure 12. Infinite gain margin and 80.2° phase margin using full state feedback via full-ordered observer with *rule of thumb* controller gains. (a) Root locus; and (b) Bode plot.

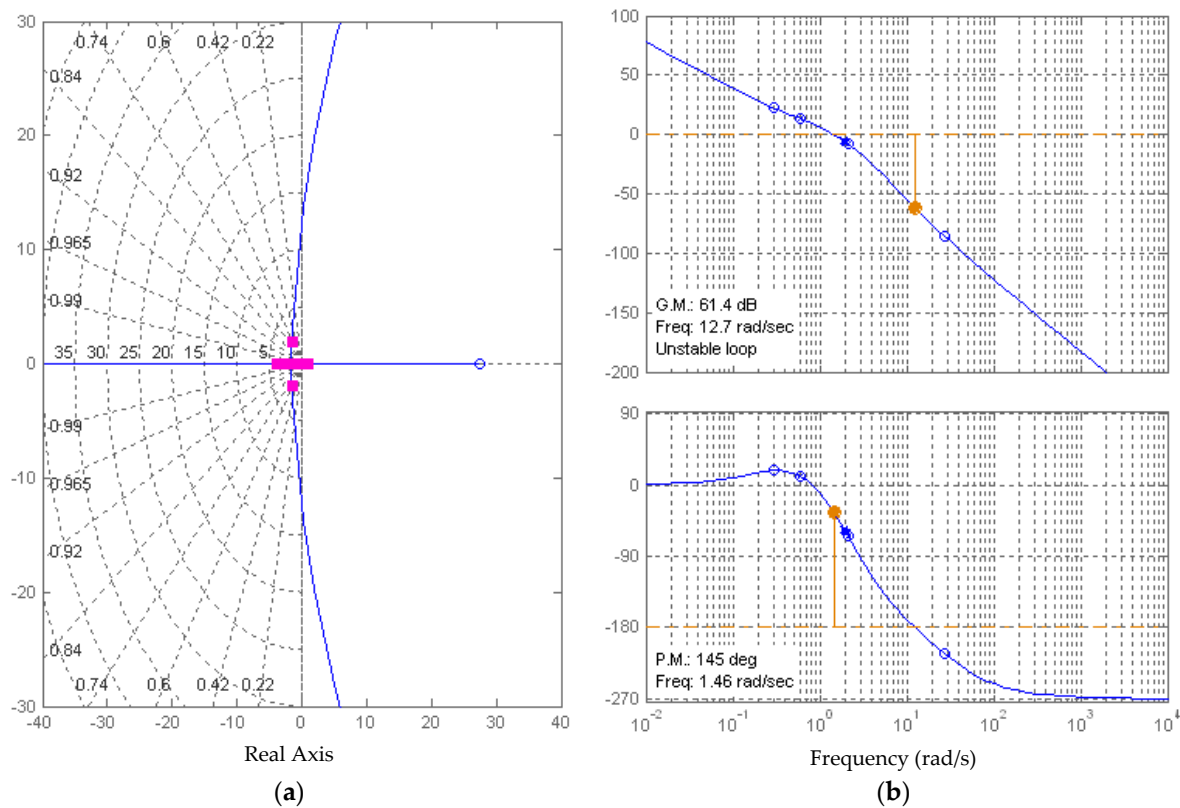


Figure 13. The 61.4 degree gain margin and 145 degree phase margin using a reduced-order observer (both rule of thumb gains for half-controller $t_c = 0.5$, and compensator with rule of thumb gains ($t_c = 1$)). (a) Root locus; and (b) Bode plot.

2.4. Tracking Systems and Feed-Forward Control in the Presence of Constant Disturbance Currents

This section evolves the earlier developed system equations and performance analysis by adding non-quiescent conditions, in particular an introduction of a lateral underwater ocean current with an absolute velocity, v_0 , requiring a modification of the system equations to add the lateral current to Equation (4) resulting in Equation (30):

$$\dot{y} = \sin\psi + v\cos\psi + v_0 \tag{30}$$

2.4.1. Analysis of Disturbed System in Ocean Currents via State Equations and Simulations

Using the controller (Equation (19)) and the modified system equations where Equation (4) is replaced by Equation (29), and applying the final value theorem: $f(t)_{t \rightarrow \infty} = sF(s)_{s \rightarrow 0}$, a steady state value $1/\omega+1$ has some variable quantity added to unity for various v_0 . Thus, steady-state errors exist in all cases with such disturbances, which is verified by simulations depicted in Figures 14 and 15 using gain values from the *rule of thumb* (ROT) for the unity time constant. The steady-state errors are directly proportional to the disturbance magnitude. Figure 8 displays the maximum rudder deflection for the maximal lateral ocean current in the study (to verify the control design this continues to remain less than 0.4 radians).

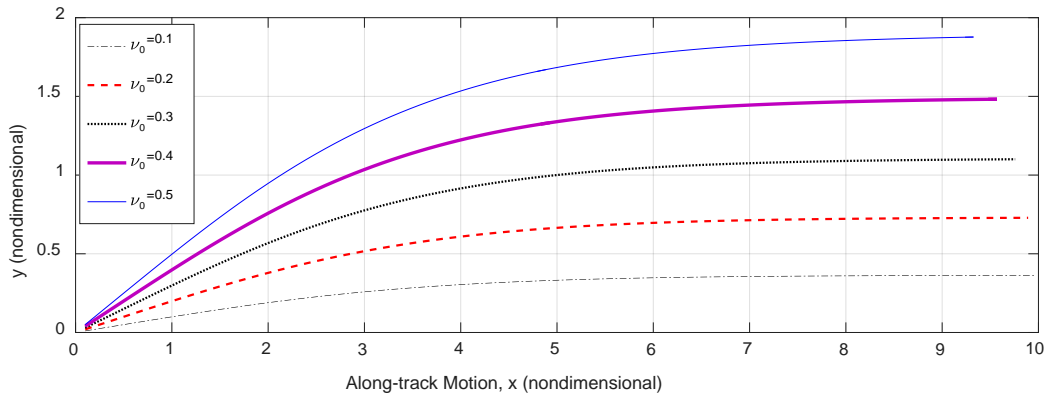


Figure 14. Steady-state position error for various lateral underwater ocean currents.

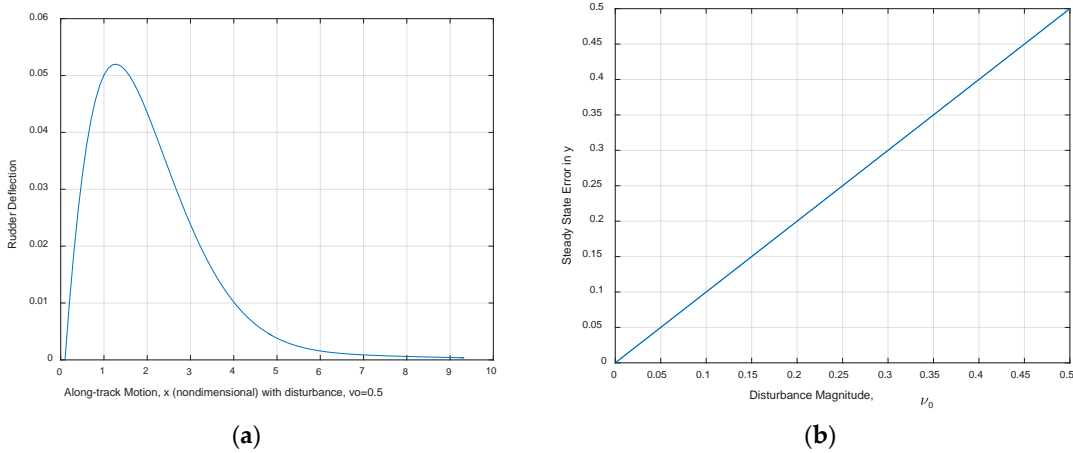


Figure 15. Feedback alone is unable to counter the constant lateral underwater ocean currents. (a) Rudder deflection, $v_0 = 0.5$; and (b) steady state error vs. v_0 .

2.4.2. Elimination of Steady-State Error Using Feed-Forward Control

The control law is modified to $\{u\}_{feedforward} = \{\delta\} = -K_1v - K_2r - K_3\psi - K_4y - K_0$ in order to eliminate the steady-state error, where K_0 is chosen to ensure zero steady-state error, where the feedback gains are chosen by the *rule of thumb*, and the results are displayed in Figures 16 and 17.

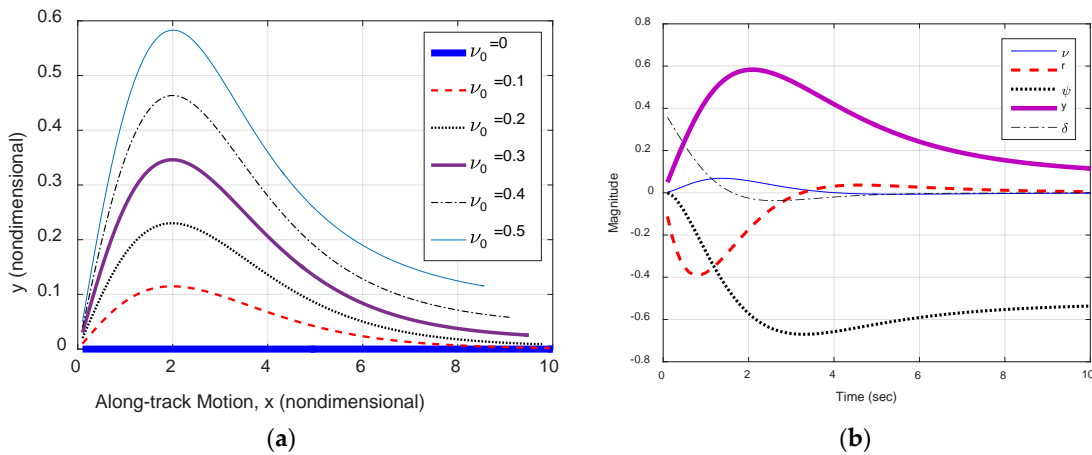


Figure 16. Feed-forward element included to counter constant lateral underwater ocean currents. (a) Rudder deflection, $v_0 = 0.5$; and (b) all states when $v_0 = 0.5$.

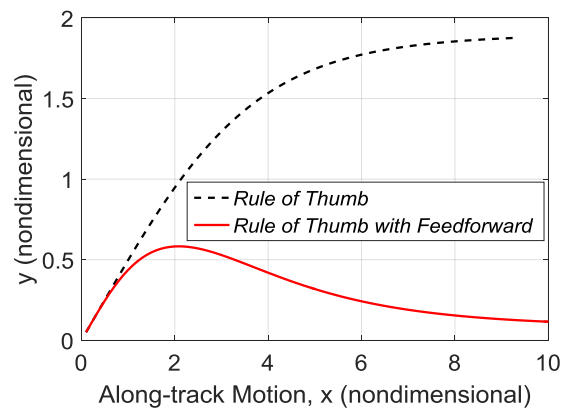


Figure 17. Comparison: feedback control with and without feed-forward ($v_0 = 0.5$).

2.5. Disturbance Estimation with Reduced-Order Observer and Integral Control

Section 2.4 demonstrated feed-forward control effectively countered the disturbance currents, but the current was presumed to be known. To be truly effective, the reduced-order observer is next augmented to include estimation of the unknown disturbance current velocity \hat{v}_c , where the observer now estimates the disturbance current velocity, the lateral sway velocity, v , the lateral deviation (cross-track error), y , and the heading angle, ψ . Figure 18a,b displays the estimates of the unknown current for two current velocity conditions: $\hat{v}_{c1} = v_{est1} = 0.1$ and $\hat{v}_{c2} = v_{est2} = 0.5$, respectively, while Figure 18c,d display the y and ψ states for each current velocity condition. Notice how large rudder deflections modify the heading angle to the command-tracking value which counters the disturbance current (sometimes referred to as “crabbing”), and after establishing the crab heading angle, the rudder deflection shifts towards zero, illustrating the effectiveness of command tracking.

Figure 19 displays all the states versus time in seconds and also the trajectory when a worst-case unknown disturbance current $v_c = 0.5$ is applied and estimated by the reduced-order observer where the observer gains are solutions to the linear quadratic Gaussian optimization. Meanwhile Figure 20 displays the results in cases utilizing command tracking with reduced order observer and with command: $\psi = -0.5$ and sinusoidal disturbance current $v_c(0) = A\sin(0.1t)$, but no disturbance estimation or feed-forward, while Figure 20 uses disturbance estimation, feed-forward, and rule of thumb gains. Figure 21 displays utilization of command tracking with reduced order observer, with command: $\psi = -0.5$, sinusoidal disturbance current $v_{c0} = A\sin(0.1t)$, disturbance estimation, and feed-forward and rule of thumb gains. Lastly, Figure 22 displays the performance of reduced-order observers, which is especially useful in instances of limited at-sea computational capabilities.

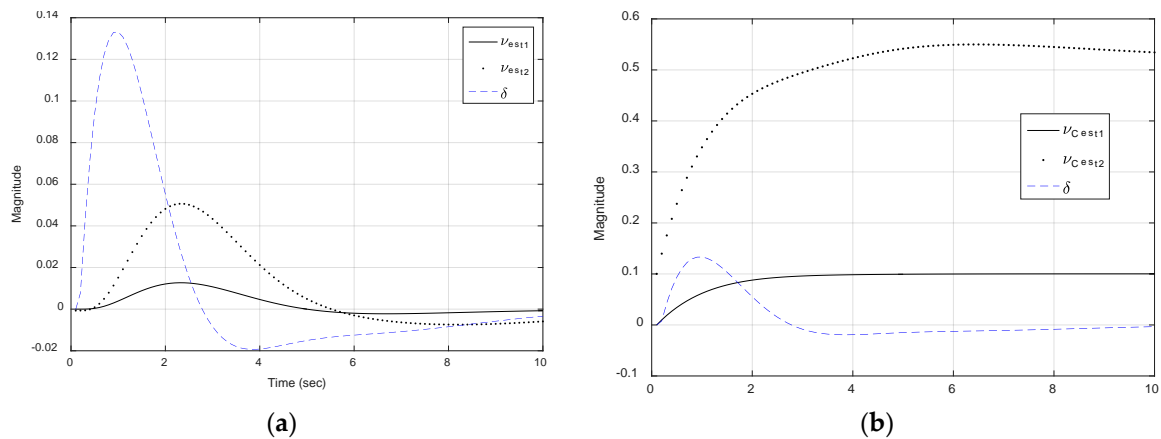


Figure 18. Cont.

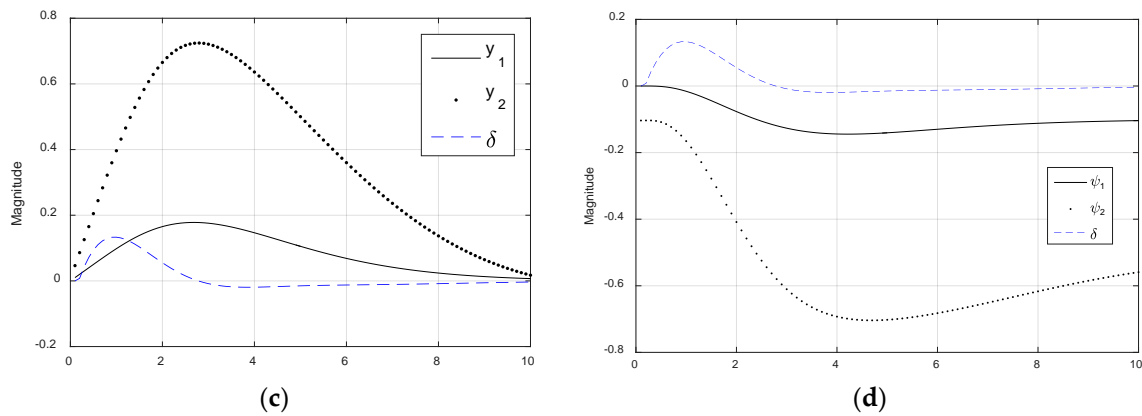


Figure 18. Reduced-order observer state estimates versus time (seconds) for two disturbance currents $v_{c0} = [0.1 \ 0.5]$, where Δ is the rudder deflection using these estimates when the worst-case disturbance current is applied. (a) Sway velocity; (b) disturbance current; (c) lateral deviation (cross-track error); and (d) heading angle.

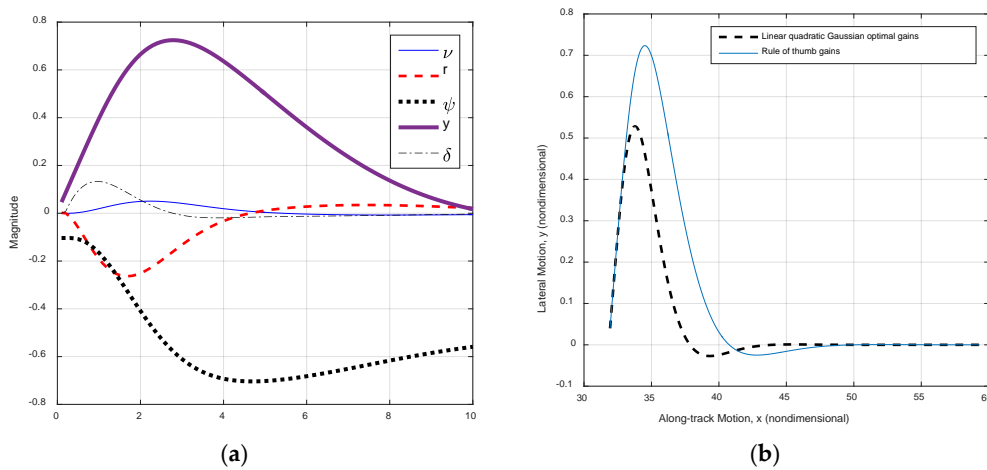


Figure 19. Performance with disturbance estimation and command tracking using LQR and *rule of thumb* gains in a reduced-order observer, and command tracking to $\psi = -0.5$ amidst a constant disturbance current $v_c = 0.5$. (a) States; and (b) trajectory.

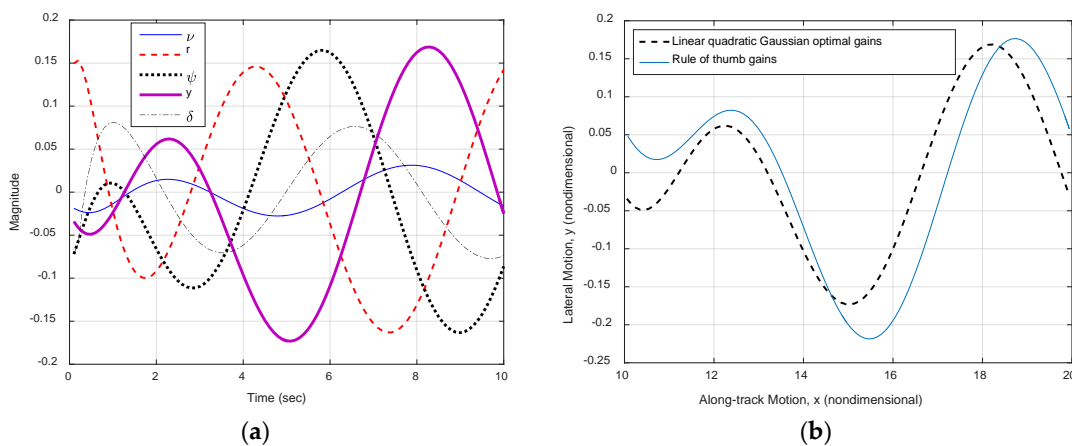


Figure 20. Utilization of command tracking with reduced order observer, with command: $\psi = -0.5$ and sinusoidal disturbance current $v_{c0} = A \sin(0.1t)$, but no disturbance estimation or feed-forward. (a) All states vs. time (seconds); and (b) trajectory.

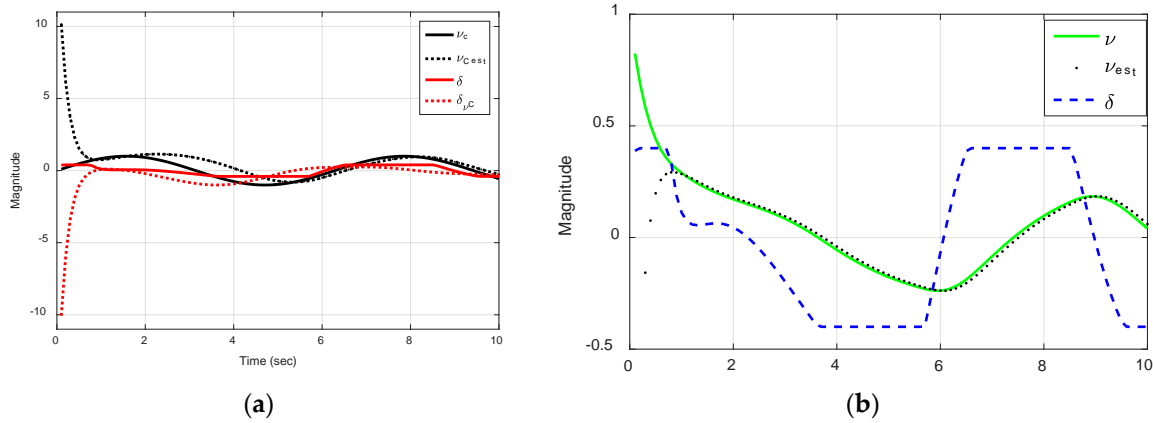


Figure 21. Utilization of command tracking with reduced order observer, with command: $\psi = -0.5$, sinusoidal disturbance current $v_{c_0} = A\sin(0.1t)$, disturbance estimation, and feed-forward and rule of thumb gains.

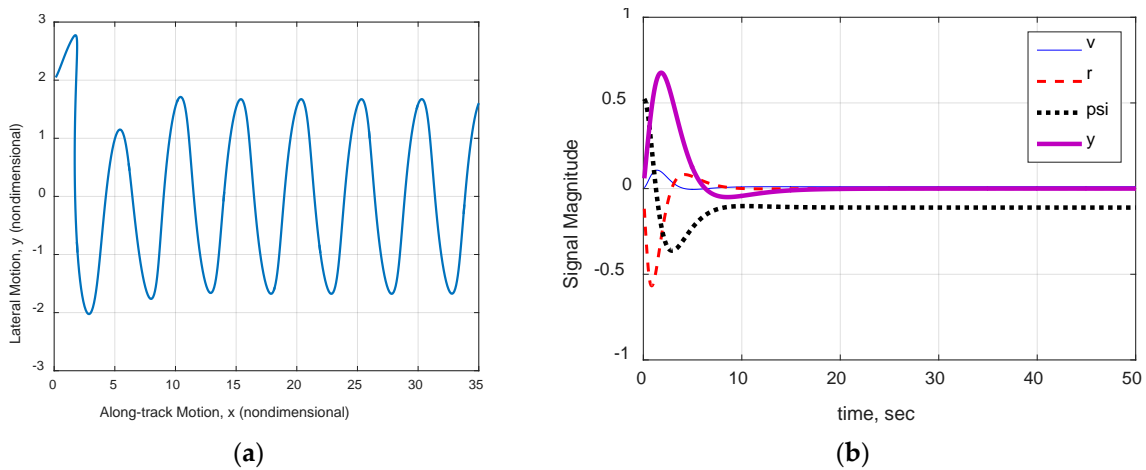


Figure 22. Utilization of command tracking with reduced order observer, with command: $\psi = -0.5$ and sinusoidal disturbance current $v_{c_0} = A\sin(0.1t)$. (a) With disturbance estimation (and feed-forward), reduced order observer; and (b) with integral control, but no disturbance estimation or feed-forward.

2.6. Waypoint Guidance

A simple line-of-sight guidance routine was employed based on fixing waypoints through a minefield in order to navigate to a specified point and safely return home. The coordinates are fed to a logic determining when to turn per Equation (31), where d is the distance to the waypoint, and the heading command was autonomously calculated per Equation (32):

$$\text{Turn if : } \sqrt{(x_c - x)^2 + (y_c - y)^2} \leq d \tag{31}$$

$$\psi_{\text{command}} = K \tan^{-1} \left(\frac{y_c - y}{x_c - x} \right) \tag{32}$$

Particular attention is brought to the inverse tangent calculation, since quadrants must be preserved in the calculation since the vehicle will navigate in 360 degrees.

3. Results

The following paragraphs mirror Section 2 above to provide a concise description of the simulation experiments to provide a concise and precise description of the experimental results,

their interpretation, as well as the experimental conclusions that can be drawn in each sub-topic introduced and developed so far. Some new developments naturally follow in the paragraphs of the results in response to the lessons learned.

3.1. System Dynamics

Some basic lessons come from a brief analysis of the uncontrolled system dynamics. The open loop plant equations are potentially unstable (at least persistently oscillatory) with respect to only the bow rudder, while the relationship can be stable with respect to the stern rudder alone. *Can be stable* is exaggerated to emphasize the presence of pole-zero cancellation, which is an unwise practice (especially in this instance with both poles and zeros at the origin on the stability boundary) unless the estimates for the constants in the system equations are very well known. The analysis of the dynamics also revealed the bow rudder was least relatively-effective at maneuvering alone when compared to the stern rudder, however, the bow rudder does enhance vehicle maneuverability when used together with the stern rudder as a “scissored-pair” where the sign of the maneuver angle is opposite for each rudder. This “scissored-pair” constraint simplified the many-in-many-out (MIMO) control design, allowing the design engineer to treat the system as a single-in-single-out (SISO) design, since one rudder’s deflection becomes a dependent variable constrained to the other rudder’s deflection.

3.2. Control Law Design

Baseline proportional-derivative control designs effectively stabilized the dynamics, but were ineffective in the presence of a constant lateral open ocean current. Gains selected by *rule of thumb* performed similar to the linear-quadratic optimal control designs, so this underwater vehicle control could be designed at sea with rudimentary math in instances when higher level computational abilities are not available. Augmentation of the control including gains tuned to reject the constant current proved effective, but required the current to be measured to permit the control component to be properly tuned. Furthermore, when the lateral disturbance current had sinusoidal variation, the controller was rendered ineffective in rejecting the disturbance.

3.3. Observer Design

The submersible vehicle’s system equations were verified observable by calculation of a full-ranked observability matrix in Section 2.3. A full state observer was designed first to permit vehicle control with “full state feedback”, yet without directly measuring velocity. Observer gains may be tuned using classical methods in the general spirit of duality between controller and observers. Their dual nature also permits the matrix Riccati equation to produce optimal gains for a linear-quadratic cost function that exclusively emphasizes state estimation error, unlike the controller optimization where the cost function balanced control effort with state error. State observers permit the vehicle operator to have smooth, calculated estimates of all states at all times, which proves useful in the event of sensor interruptions or failures, and reduced-ordered observers may be used in instances where computations on-board the vehicle must be limited, for example to minimize computer size, weight, and/or power.

Especially in light of naturally occurring (roughly) sinusoidal variations in ocean current, the system equations were augmented to include the presumed-unknown disturbance as a state.

3.4. Tracking Systems and Feed-Forward Control in the Presence of Disturbance Currents

Simple feed-forward control elements proved effective against known or estimated constant lateral disturbance currents by allowing the vehicle to autonomously perform “set-and-drift” principles where a highly-trained helmsman would turn the bow of a ship into a current, but the simple feed-forward elements were ineffective at countering currents with sinusoidal variation. In the set and drift principle the heading is de facto non-zero, so the vehicle cannot simultaneously maintain center-pointing while countering the disturbance. If such a requirement were added, designers must decouple the

scissored-pair rudder constraint and design the rudder commands separately to simultaneously counter the disturbance while maintaining centerline pointing.

3.5. Disturbance Estimation and Integral Control

Full-ordered observers effectively estimated constant and sinusoidal disturbance currents and proved useful in the control designs for feed-forward control, but, furthermore, reduced-ordered observers were applied in cases where disturbances were forces and moments and feed-forward control was not used. Integral control was used instead to drive the steady-state error to zero where sufficiently large time constants were used for the integrator, i.e., the fifth pole in the pole placement control must be less negative than the other poles.

3.6. Fully-Assembled System Demonstration

In light of all these results, a fully-assembled control system was used to navigate the proper mathematical models of the *Phoenix* autonomous submersible vehicle through a simulated $200\text{ m} \times 500\text{ m}$ minefield in the presence of unknown ocean currents. The field was populated randomly with 30+ mines, and the vehicle successfully traversed the minefield in the presence of an unknown 0.5 m/s current with a miss distance from the nearest mine not less than 5 m , navigating from the starting point to pass within 0.5 m of a commanded en route point at sea, and then return to the start point. The outer loop controller used line-of-sight guidance to provide heading commands to the inner loop, and the inner loop controller was an output-feedback heading controller. Two control strategies both proved effective: linear-quadratic Gaussian, and approximate optimal pole-placement by *rule of thumb*. In the linear-quadratic Gaussian case, both the controller gains and observer gains were selected by optimization of the respective matrix Riccati equation. Figure 23 displays the completed maneuver where each dot displays the location of a randomly-placed mine. Full state feedback was achieved with state observers via the certainly equivalence principle and the states were utilized in a proportional-derivative-integral feedback control architecture. Detailed outputs and figures of merit are plotted in Figures 24–28, including performance of a second transit of the minefield for validation purposes.

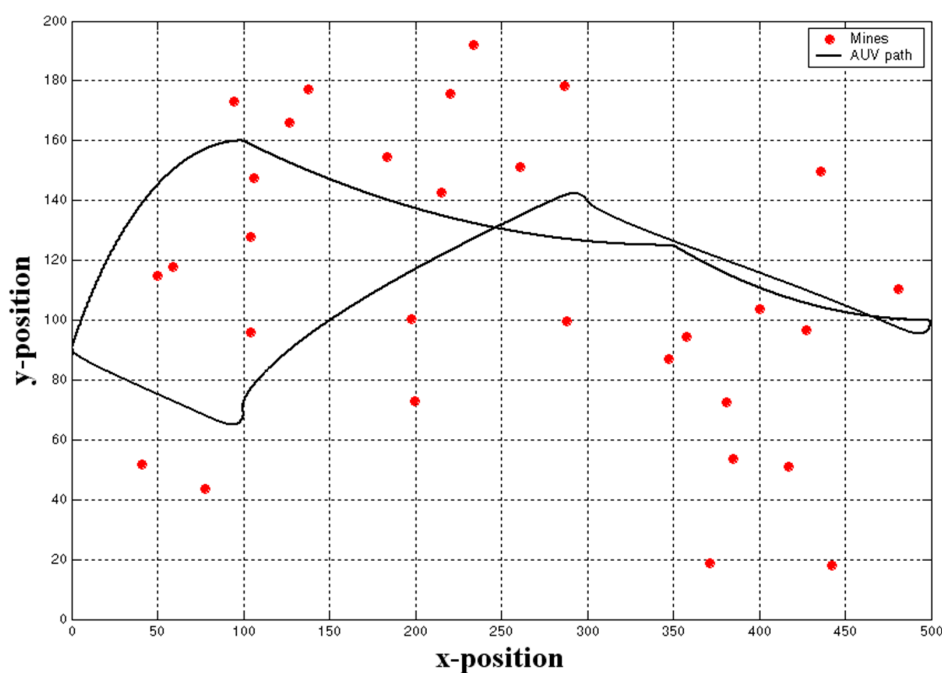


Figure 23. Navigation through simulated field of 30 randomly placed mines in -0.5 m/s current with linear quadratic Gaussian PID controller and full-state observer.

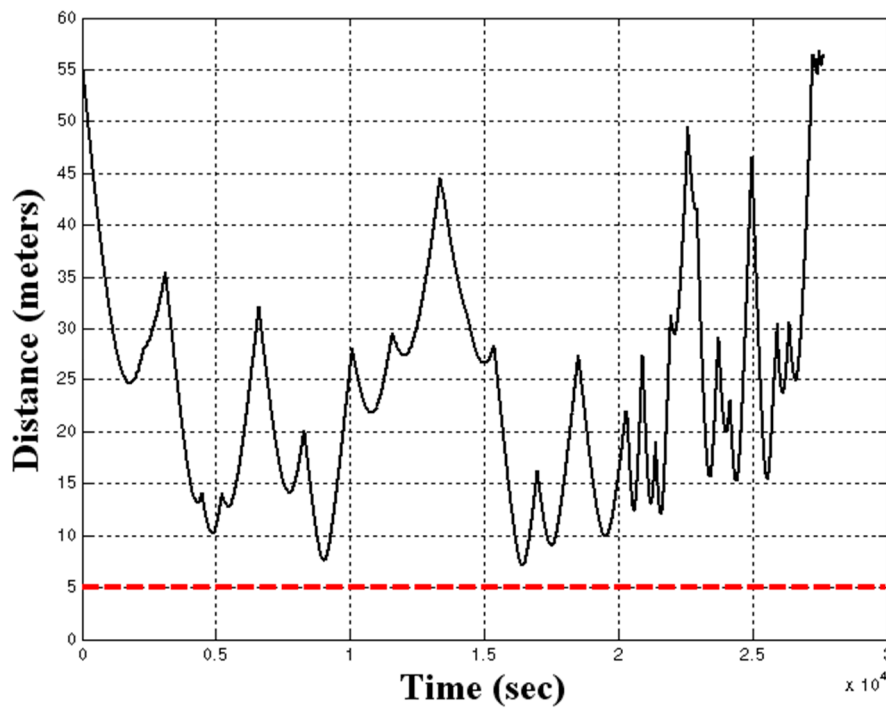


Figure 24. Continuous distance (meters) to closest mine with Linear quadratic Gaussian optimized PID controller and *full-state* observer versus time (seconds).

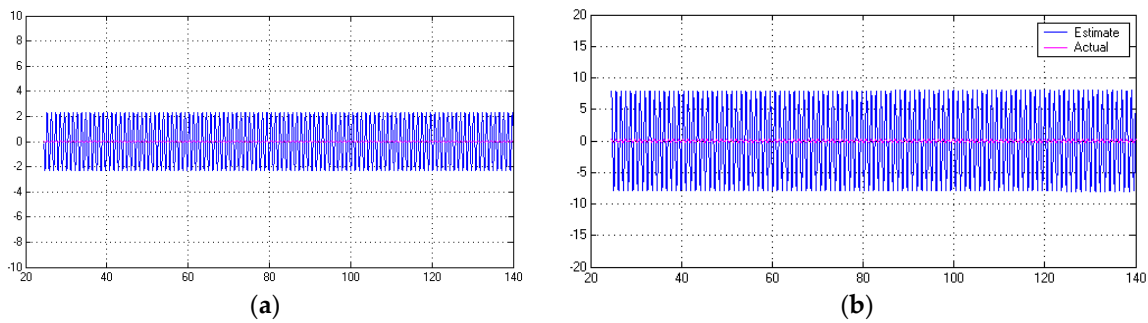


Figure 25. Linear quadratic (Gaussian) optimal observer convergence with actual value in light-pink near zero, while estimates are depicted oscillating in blue. (a) State v ; and (b) state r .

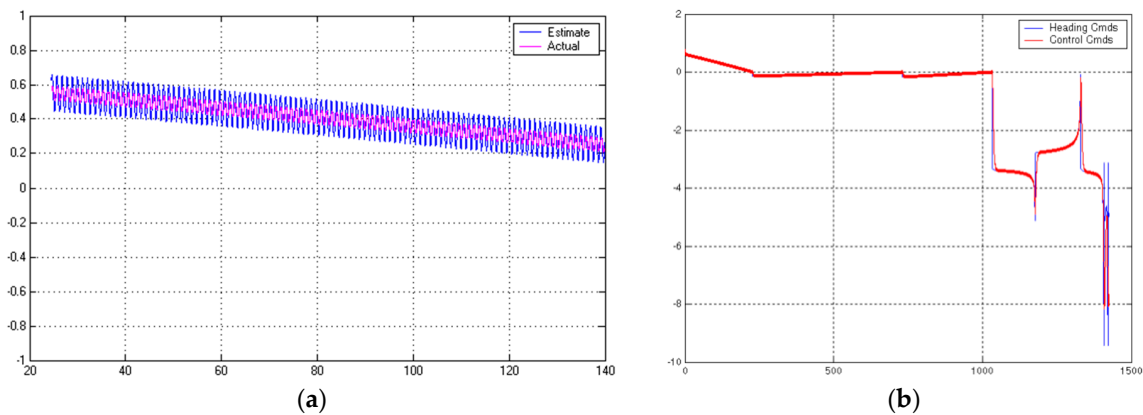


Figure 26. Linear quadratic (Gaussian) optimal observer convergence. (a) State ψ ; and (b) command tracking (radians) versus time (seconds).

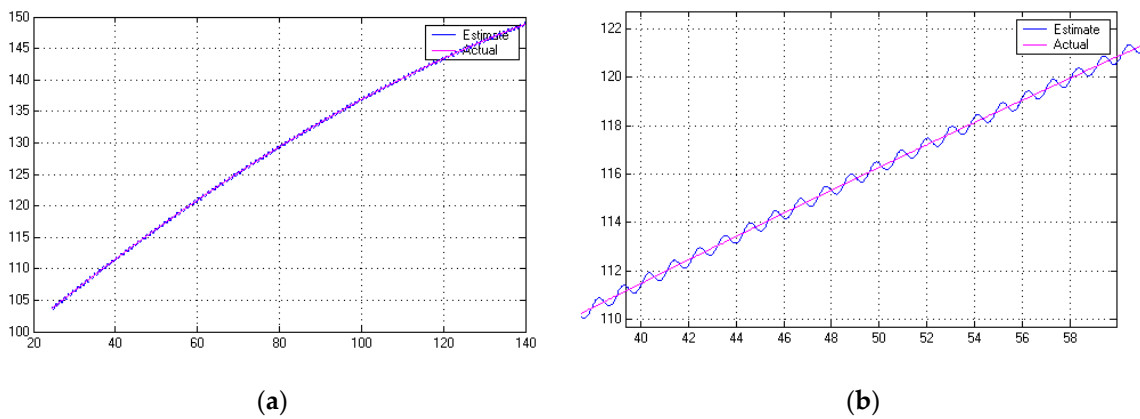


Figure 27. Linear quadratic (Gaussian) optimal observer convergence of y ; (a) State y ; (b) State.

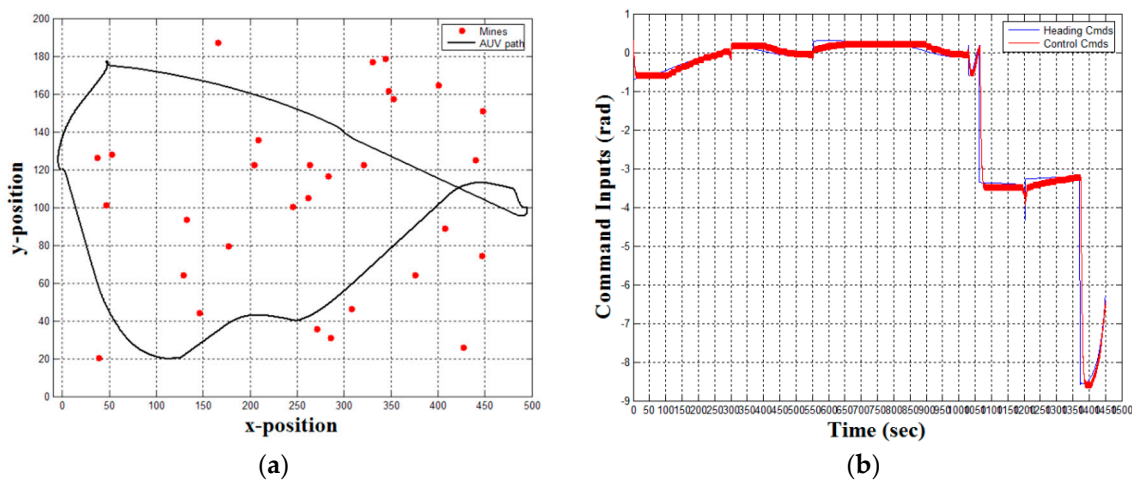


Figure 28. Validation trajectory through simulated field of 30 randomly placed mines in -0.5 m/s current with linear quadratic Gaussian optimized PI controller and *reduced-ordered* observer. (a) Second trajectory (results validation); and (b) heading command tracking.

4. Discussion

The results of this study establish both classical and modern control paradigms to guide autonomous submersible vehicles through obstacles in unknown ocean currents. Assuming the availability of the recent technologies cited in the Introduction, methods were investigated to use these technologies to guide a submersed vehicle along a preplanned path through a field of randomly placed obstacles. The constituent technologies investigated in Section 2 were then combined in a fully-assembled system demonstration in Section 3 (Results), where the figure of merit used to assess the efficacy of the proposed methods is the maintenance of the miss distance from submersible objects in ocean currents. The conclusions from the experiments follow: both elegant and simplified autonomous controls proved effective (achieving consistent miss distance from mines greater than the goal of five meters), making this technology immediately accessible to low-end technology implementations. The results are consistent with the significant body of literature on motion mechanics in the presence of unknown disturbances with the added complication of restricted path planning due to randomly-placed obstacles, where mines were used in this study driving an additional requirement of minimum safe distance for obstacle passage. This consistency with the current literature leads to a natural direction for future research, since recent innovations in nonlinear idealized (and sometimes also adaptive) methods have recently proven to be natural extensions of technology in these fields.

These recent innovations stem from the imminent realization that the United States has been, for many years, preoccupied with low-intensity conflicts against technologically inferior opponents at a time when competitor nations have made great technological advancements in navigation and motion mechanics. The advancements in motion mechanics, as embodied in recent warhead maneuvering advancements for nuclear weapons, are exacerbated by a glaring reduction in the technical prowess of the American nuclear enterprise resulting in a very recent reinvigoration of the critical thinking abilities of the enterprise through education efforts designed to return the American enterprise to the forefront of technology in these areas. The idealized nonlinear methods are a part of the renewed education effort, and accompanying the renewed emphasis in this direction, the sequel to this manuscript should include an investigation of idealized nonlinear and adaptive methods with a direct comparison to the current state-of-the-art including time-optimal control methods. The implications of the current American deficit expanded in this year's nuclear posture review indicate a steady funding source for such education in the near future.

Immediate future research will attempt to improve obstacle avoidance performance using nonlinear Feed-forward methods from the referenced literature when they show real promise. Another area of future research is the investigation of the limiting conditions of system parameter variation under which the rule-of-thumb technique remains effective, although it is assumed to be generically effective, since the system time constant method would be appropriately applied to any system equation. The key to effectiveness lies in online knowledge of the parameter variations, which is a natural extension of the nonlinear feed-forward methods to be investigated. The impetus for this research is the realization the United States has been preoccupied in the Middle East [26] and has lost the technical edge. In light of recent diplomatic failures [27] together with blatant signs of an insufficiently educated enterprise [28,29], and coupled with a resurgently aggressive defense posture [30,31], new efforts seek to elevate the critical thinking abilities of the enterprise with focused education including the topics elaborated in this manuscript amongst many others [32–36] in hopes that future enterprise members will be increasingly well prepared for highly technical defense missions [37–39]. A natural sequel to this manuscript would utilize most recent advancements in vehicle kinematics [40] in addition to the aforementioned methods ([32–36] in particular), which comprise nonlinear mathematical amplifications of the linear methods utilized here, and the impacts on critical thinking of enterprise members should be assessed after these methods are incorporated into a standard curriculum.

Author Contributions: Conceptualization by A.H., foremost, and then K.B. and T.S. afterwards; methodology by A.H.; software by K.B. and T.S.; validation by I.K., T.S., and K.B.; formal analysis by T.S. and K.B.; writing—original draft preparation by T.S.; writing—review and editing by T.S.; research supervision by I.K. Authorship has been limited to those who have contributed substantially to the work reported.

Funding: This research received no external funding. No sources of funding apply to the study. Grants were not received in support of our research work. No funds were received for covering the costs to publish in open access, instead this was an invited manuscript to the special issue.

Conflicts of Interest: The authors declare no conflict of interest.

References

1. Naval Postgraduate School Website for Consortium for Robotics and Unmanned Systems Education and Research (CRUSER). Available online: <http://auvac.org/people-organizations/view/241> (accessed on 23 May 2018).
2. Brutzman, D.; Healey, A.J.; Marco, D.B.; McGhee, R.B. The Phoenix Autonomous Underwater Vehicle. In *AI Based Mobile Robots*; Kortenkamp, D., Bonasso, R.P., Murphy, R.R., Eds.; MIT/AAAI Press: Cambridge, MA, USA, 1998.
3. Naval Postgraduate School Website for Consortium for Robotics and Unmanned Systems Education and Research (CRUSER). Available online: <https://my.nps.edu/web/cavr/auv> (accessed on 23 May 2018).

4. Ogata, K. *Modern Control Engineering*, 4th ed.; Prentice-Hall: Upper Saddle River, NJ, USA, 2002; pp. 779–790, ISBN 0-13-060907-2.
5. Marco, D.B.; Healey, A.J. Surge Motion Parameter Identification for the NPS Phoenix AUV. In *Proceedings International Advanced Robotics Program IARP 98*; University of South Louisiana: Baton Rouge, LA, USA, 1998; pp. 197–210.
6. Kenny, T.; Sands, T. Experimental piezoelectric system identification. *J. Mech. Eng. Autom.* **2017**, *76*, 179–195. [[CrossRef](#)]
7. Sands, T. Nonlinear-adaptive mathematical system identification. *Computation* **2017**, *5*, 47–59. [[CrossRef](#)]
8. Kenny, T.; Sands, T. Experimental Sensor Characterization. *J. Space Explor.* **2017**, *7*, 140.
9. Sands, T. Space System Identification Algorithms. *J. Space Explor.* **2017**, *6*, 138.
10. Armani, C.; Sands, T. Analysis, correlation, and estimation for control of material properties. *J. Mech. Eng. Autom.* **2018**, *8*, 7–31. [[CrossRef](#)]
11. Wu, N.; Wu, C.; Ge, T.; Yang, D.; Yang, R. Pitch Channel Control of a REMUS AUV with Input Saturation and Coupling Disturbances. *Appl. Sci.* **2018**, *8*, 253. [[CrossRef](#)]
12. He, B.; Zhang, H.; Li, C.; Zhang, S.; Liang, Y.; Yan, T. Autonomous Navigation for Autonomous Underwater Vehicles Based on Information Filters and Active Sensing. *Sensors* **2011**, *11*, 10958–10980. [[CrossRef](#)] [[PubMed](#)]
13. Yan, Z.; Wang, L.; Zhang, W.; Zhou, J.; Wang, M. Polar Grid Navigation Algorithm for Unmanned Underwater Vehicles. *Sensors* **2017**, *17*, 1599. [[CrossRef](#)]
14. Wang, J.; Li, B.; Chen, L.; Li, L. A Novel Detection Method for Underwater Moving Targets by Measuring Their ELF Emissions with Inductive Sensors. *Sensors* **2017**, *17*, 1734. [[CrossRef](#)] [[PubMed](#)]
15. Eren, F.; Pe’eri, S.; Thein, M.; Rzhhanov, Y.; Celikkol, B.; Swift, M.R. Position, Orientation and Velocity Detection of Unmanned Underwater Vehicles (UUVs) Using an Optical Detector Array. *Sensors* **2017**, *17*, 1741. [[CrossRef](#)] [[PubMed](#)]
16. Zhang, W.; Wei, S.; Teng, Y.; Zhang, J.; Wang, X.; Yan, Z. Dynamic Obstacle Avoidance for Unmanned Underwater Vehicles Based on an Improved Velocity Obstacle Method. *Sensors* **2017**, *17*, 2742. [[CrossRef](#)] [[PubMed](#)]
17. Kim, J.J.; Agrawal, B.; Sands, T. 2H Singularity free momentum generation with non-redundant control moment gyroscopes. In *Proceedings of the 45th IEEE Conference on Decision and Control*, San Diego, CA, USA, 13–15 December 2006; pp. 1551–1556. [[CrossRef](#)]
18. Kim, J.J.; Agrawal, B.; Sands, T. Control moment gyroscope singularity reduction via decoupled control. In *Proceedings of the IEEE Southeastcon 2009*, Atlanta, GA, USA, 5–8 March 2009; pp. 1551–1556. [[CrossRef](#)]
19. Sands, T.; Kim, J.J.; Agrawal, B. Nonredundant single-gimbaled control moment gyroscopes. *J. Guid. Control Dyn.* **2012**, *35*, 578–587. [[CrossRef](#)]
20. Kim, J.J.; Agrawal, B.; Sands, T. Experiments in Control of Rotational Mechanics. *Int. J. Autom. Control. Intell. Syst.* **2016**, *2*, 9–22.
21. Agrawal, B.; Kim, J.J.; Sands, T. Method and Apparatus for Singularity Avoidance for Control Moment Gyroscope (CMG) Systems without Using Null Motion. U.S. Patent 9,567,112, 2017.
22. Agrawal, B.; Kim, J.J.; Sands, T. Singularity Penetration with Unit Delay (SPUD). *Mathematics* **2018**, *6*, 23–38. [[CrossRef](#)]
23. Lu, D.; Chu, J.; Cheng, B.; Sands, T. Developments in angular momentum exchange. *Int. J. Aerosp. Sci.* **2018**, *6*, 1–7. [[CrossRef](#)]
24. Thornton, B.; Ura, T.; Nose, Y. Wind-up AUVs Combined energy storage and attitude control using control moment gyros. In *Proceedings of the Oceans 2007*, Vancouver, BC, Canada, 29 September–4 October 2007. [[CrossRef](#)]
25. Thornton, B.; Ura, T.; Nose, Y. Combined energy storage and three-axis attitude control of a gyroscopically actuated AUV. In *Proceedings of the Oceans 2008*, Quebec City, QC, Canada, 15–18 September 2008. [[CrossRef](#)]
26. Sands, T. Strategies for combating Islamic state. *Soc. Sci.* **2016**, *5*, 39. [[CrossRef](#)]
27. Mihalik, R.; Sands, T. Outcomes of the 2010 and 2015 nonproliferation treaty review conferences. *World J. Soc. Sci. Humanit.* **2016**, *2*, 46–51. [[CrossRef](#)]
28. Camacho, H.; Mihalik, R.; Sands, T. Education in Nuclear Deterrence and Assurance. *J. Def. Manag.* **2017**, *7*, 166. [[CrossRef](#)]

29. Mihalik, R.; Camacho, H.; Sands, T. Continuum of learning: Combining education, training and experiences. *Education* **2017**, *8*, 9–13. [[CrossRef](#)]
30. Camacho, H.; Mihalik, R.; Sands, T. Theoretical Context of the Nuclear Posture Review. *J. Soc. Sci.* **2018**, *14*, 124–128. [[CrossRef](#)]
31. Mihalik, R.; Camacho, H.; Sands, T. U.S. Nuclear Posture Review—Kahn vs. Schelling. *Soc. Sci.* **2018**, *14*, 145–154.
32. Sands, T. Physics-based control methods. In *Advances in Spacecraft Systems and Orbit Determination*; InTech: London, UK, 2012.
33. Nakatani, S.; Sands, T. Simulation of spacecraft damage tolerance and adaptive controls. In Proceedings of the 2014 IEEE Aerospace Conference, Big Sky, MT, USA, 1–8 March 2014; pp. 1–16. [[CrossRef](#)]
34. Nakatani, S.; Sands, T. Autonomous damage recovery in space. *Int. J. Autom. Control. Intell. Syst.* **2016**, *2*, 22–36.
35. Cooper, M.; Heidlauf, P.; Sands, T. Controlling Chaos—Forced van der Pol Equation. *Mathematics* **2017**, *5*, 70–80. [[CrossRef](#)]
36. Nakatani, S.; Sands, T. Battle-damage tolerant automatic controls. *Elec. Electr. Eng.* **2018**, *8*, 10–23. [[CrossRef](#)]
37. Sands, T. Satellite electronic attack of enemy air defenses. In Proceedings of the IEEE Southeastcon 2009, Atlanta, GA, USA, 5–8 March 2009; pp. 434–438. [[CrossRef](#)]
38. Sands, T. Space mission analysis and design for electromagnetic suppression of radar. *Int. J. Electromagn. Appl.* **2018**, *8*, 1–25. [[CrossRef](#)]
39. Nakatani, S.; Sands, T. Eliminating the existential threat from North Korea. *Sci. Technol.* **2018**, *8*, 11–16. [[CrossRef](#)]
40. Smeresky, B.; Rizzo, A.; Sands, T. Kinematics in the Information Age. *Mathematics* **2018**, accepted.



© 2018 by the authors. Licensee MDPI, Basel, Switzerland. This article is an open access article distributed under the terms and conditions of the Creative Commons Attribution (CC BY) license (<http://creativecommons.org/licenses/by/4.0/>).